universität wien

BACHELORARBEIT / BACHELOR THESIS

Titel der Bachelorarbeit / Title of the Bachelor Thesis

Highly siderophile element budget and osmium isotopes of Paleoarchean spherules
- a spherule vs. matrix investigation -

verfasst von / submitted by

Olivier Karl Anton Heldwein

angestrebter akademischer Grad / in partial fulfilment of the requirements for the degree of

Bachelor of Science (BSc)

Wien, 2017 / Vienna 2017

Studienkennzahl lt. Studienblatt / degree programme code as it appears on the student record sheet:	A 033 615
Studienrichtung lt. Studienblatt / degree programme as it appears on the student record sheet:	Bachelorstudium Erdwissenschaften UG2002
Betreut von / Supervisor:	Dr. Toni Schulz

Abstract

Distal impact ejecta, consisting of millimeter-sized glassy spherules, comprise the only remnants of the Archean impact record. Studying these spherule layers gives insights into the early meteorite bombardment of the Earth, its effects on the early crust, ocean, atmosphere, and life, and into the complex processes in impact vapor plumes, where these spherules are thought to have formed. Only a few dozens of Archean spherule layers are known so far. Thus, the finding of possibly up to eight new layers in the recent BARB5 drill core from Barberton Greenstone Belt (South Africa) offers a unique opportunity to delve deeper into this subject. This study concentrates on the spatial distribution of the carrier phase(s) of the meteoritic component. For this reason, a sample from the uppermost of the newly discovered layers (layer E) has been separated into spherules and matrix and investigated regarding its highly siderophile element budget (Re, Os, Ir, and Pt) and $^{187}Os/^{188}Os$ isotope systematics. Based on spherule-matrix (groundmass) separates, meteoritic components have recently been detected in all BARB5 spherule layers but none of these data were performed on pure spherule separates.

Using highly siderophile element abundances and the $^{187}Os/^{188}Os$ tool, this study presents confirmation for meteoritic components within both separates. The spherules exhibit Os and Ir contents of 83.78 ppb and 70.29 ppb, respectively, and a $^{187}Os/^{188}Os$ ratio of 0.10578 ± 0.00029. These values are comparable to those found in the matrix (171.21 ppb Os; 205.46 ppb Ir; 0.10767 ± 0.00017 $^{187}Os/^{188}Os$ ratio), providing evidence for the occurrence of non-spherule related carrier phase(s) of the extraterrestrial component.

Kurzfassung

Distale Impakt-Auswürfe in Form von millimetergroßen Glas-Sphärulen sind die einzigen Zeugen der Impaktgeschichte des Archaikums. Das Studium dieser Ablagerungen erlaubt Einblicke in das Meteoritenbombardement der jungen Erde und dessen Auswirkungen auf die gerade entstehende Erdkruste, die Ozeane, die Atmosphäre und die Entwicklung des Lebens sowie in die komplexen Prozesse in den Impakt-Gaswolken, in denen diese Sphärulen entstanden sein sollen. Nur wenige Dutzend Sphärulenlagen aus dieser Zeit sind bisher bekannt. Umso wichtiger ist die Entdeckung von bis zu acht neuen Sphärulenlagen in dem kürzlich gezogenen Bohrkern BARB5 aus dem Barberton Grünsteingürtel in Südafrika, da sie eine

einzigartige Gelegenheit bietet unser Wissen in diesem Gebiet zu vertiefen. In dieser Studie wird das Hauptaugenmerk auf die räumliche Verteilung der meteoritischen Komponente(n) gelegt. Zu diesem Zweck wurde eine Probe aus der obersten der eben genannten Lagen (Lage E) in Sphärulen und ihre Tonstein-Matrix getrennt und ihr Gehalt an hochsiderophilen Element (Re, Os, Ir and Pt) sowie ihre $^{187}Os/^{188}Os$ Isotopensystematik untersucht. In Sphärulen-Matrix-Separaten konnten kürzlich meteoritische Komponenten in allen untersuchten Sphärulenlagen des BARB5 Bohrkerns nachgewiesen werden, es liegen jedoch keine Daten für reine Sphärulenproben vor. Anhand von hochsiderophilen Elementen und $^{187}Os/^{188}Os$ Isotopendaten bestätigt diese Studie das Vorhandensein von meteoritischen Spuren in beiden Separaten. Die Sphärulen zeigen Ir- und Os-Konzentrationen von 83.78 ppb beziehungsweise 70.29 ppb und ein $^{187}Os/^{188}Os$ -Verhältnis von 0.10578 ± 0.00029. Diese Werte sind vergleichbar mit jenen der Matrix (171.21 ppb Os; 205.46 ppb Ir; 0.10767 ± 0.00017 $^{187}Os/^{188}Os$ Isotopenverhältnis) und liefern den Beweis, dass zumindest eine jener Phasen, die die meteoritische Komponente in sich tragen auch unabhängig von Sphärulen vorkommt.

Acknowledgements

Gratefully, I thank the following persons for their contributions in the successful completion of this thesis:

My supervisor Dr. Toni Schulz for introducing me into clean lab work, teaching me mass spectrometry and supporting me with a lot of patience in writing and reviewing this thesis. Ing. Monika Horschinegg for assistance in lab work and analysis. Univ.-Prof. Dr. Christian Koeberl for reviewing the thesis. My family for encouragement and support throughout my years of study.

Content

1.Introduction 4
1.1 The Archean impact record 4
1.2 Crater formation and impactites 5
1.3 Study area 7
1.4 The geochemistry of impactites 9
1.4.1 Moderately siderophile elements 10
1.4.2 Highly siderophile elements 10
1.4.3 The ^{187}Re- ^{187}Os isotopic system 11
1.4.4 Chromium isotopes 12
2.Samples and analytical methods 12
2.1 Samples 12
2.2 Sample preparation and analytical methods 14
2.2.1 Sample preparation (hand picking) 14
2.2.2 High pressure asher dissolution (extraction of HSEs) 15
2.2.3 Solvent extraction (separating Os from all the other HSEs) 15
2.2.4 Back extraction and micro-distillation (purifying Os) 16
2.2.5 Anion exchange chemistry (separating and purifying HSEs) 16
2.3 Mass spectrometry 17
2.3.1 Negative thermal ionization mass spectrometry 18
2.3.2 Inductively coupled plasma mass spectrometry 19
3.Results 21
3.1 Geochemistry 21
3.2 Rhenium-osmium isotope systematics 21
4.Discussion and conclusions 22
4.1 Spatial distribution of the carrier phase 22
4.2 The rhenium problem 26
4.3 Conclusions 28
Bibliography 29
List of figures 33
List of tables 33
Appendix 34
Meteoritic admixture to BARB5- layers B to E 34
Equation for isotope dilution 34
HSE column chemistry 35
Mass interferences on Os 36

Thesis objective

The highly siderophile element (HSE) and ^{187}Os isotope budget of Paleoarchean impact spherule layer samples from the recently drilled BARB5 core (Barberton Greenstone Belt, South Africa) were analyzed in order to better assess the magnitude and spatial distribution of meteoritic admixtures within the layers. Instead of analyzing bulk samples of the layers (as utilized in earlier studies), in this study, for the first time, I have separately analyzed the two main components of these samples: spherules and groundmass.

1. Introduction

1.1 The Archean impact record

Even though all other terrestrial planets and their moons are full of impact craters (Hartmann, 1977), on Earth only ~190 impact structures of various ages and sizes are known today (Earth Impact Database, 2017). Due to erosion and other geological processes more than 80% of all impact structures on Earth are younger than 500 Ma (Earth Impact Database, 2017). The oldest known impact structure, Vredefort in South Africa, has an age of 2023 ± 4 Ma (Kamo et al, 1996), and no impact structures of Archean age are known so far on Earth (see Figure 1). Such an age bias is in marked contrast to the impact record on the Moon, where a spike in the impact flux during the time period between ~3.90 and ~3.82 Ga, called late heavy bombardment (LHB), is documented in form of large impact basins (e.g., Koeberl, 2003; Ryder 1990, 2001, 2002). As the Earth has a larger diameter and a much larger gravitational cross section compared to the Moon, it must have been subjected to a higher impact flux at any given time span. The first "real" rock record of impact events on Earth are ejecta layers, dated at ~3.47 Ga, which, according to recent models, may constitute the tail-end of the LHB (e.g., Bottke et al., 2012; Goderis et al., 2013).

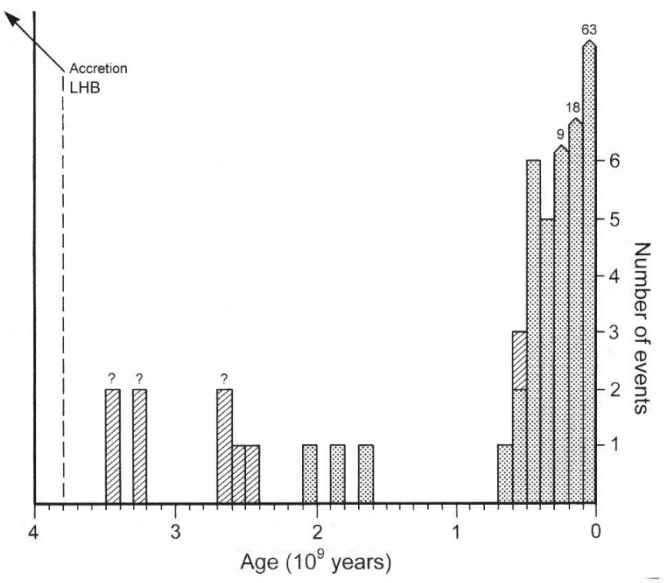

Figure 1. *Histogram of ages of known terrestrial impact structures, exemplifying the crater age bias towards the last 500 Ma. The dot-pattern indicates impact structures, whereas the hatched pattern signifies ejecta layers (from Koeberl, 2006).*

Distal impact ejecta, in the form of spherule layers, comprise the only remnants of Archean impact events (the term impactites in more generally introduced in the next chapter). At least 16 distal ejecta/spherule layers have been identified ranging from ~2.49 to ~3.47 Ga (e.g., Glass and Simonson, 2012). These Archean spherule layers are found in the 3.24 to 3.47 Ga old successions of the Barberton Greenstone Belt (BGB) in South Africa and the Pilbara Craton in Western Australia, as well as in the ~2.6 Ga Hamersley Basin in Australia and in the Monteville Formation of the Transvaal Supergroup in South Africa (e.g., Simonson, 1992, 2003; Simonson and Hassler, 1997; Simonson et al., 1993, 1998, 1999; Woodhead et al., 1998; Hassler and Simonson, 2001; Shukolyukov et al., 2002; Rasmussen and Koeberl, 2004). It should be noted, however, that the occurrence of spherules is not restricted to the Archean (Phanerozoic and Proterozoic spherule layers are also known; e.g., Glass and Simonson, 2012). The number of preserved Archean spherule layers is still relatively low when considering the much higher impact flux that can be expected during the Archean. Thus, findings of new spherule layers, such as those found in the recently recovered BARB5 and CT3 drillcores in the Barberton Greenstone Belt (South Africa), provide an outstanding opportunity to gain deeper insight into the early bombardment of the Earth.

This study presents a HSE and $^{187}Os/^{188}Os$ study of two separates from a spherule layer sample recovered from the BARB5 drill core. Before explaining the methodological approach utilized in this study and discussing the results, the basics of impact science are introduced.

1.2 Crater formation and impactites

Impact craters (which, after erosional post-impact modification are always termed "impact structures “) are classified into two morphological types: simple, bowl shaped craters (diameter < 2-4 km) and complex craters with a central uplift and or peak ring (diameter >2-4 km) are formed (Melosh, 1989). The cratering process lasts not longer than some minutes and can be divided into three main stages, which are (i) contact and compression, (ii) excavation and (iii) modification (e.g., French 1998; Koeberl 2014).

During the first phase, shockwaves and release waves propagate through the impactor and the target, leading to virtually instantaneous melting and vaporization of the impactor, which mixes with the molten and evaporated portions of the target. During

the excavation stage, complex interactions between the shock waves and the original ground surface lead to the opening of the crater by displacing and ejecting material (e.g., French 1998; Koeberl 2014). The resulting crater typically has a diameter 10 to 20 times larger than the impactor (e.g., French 1998; Koeberl 2014). Immediately after the excavation stage the third stage begins (modification). Small craters only little modification resulting simple craters with the same size as the transient cavity, while craters with a larger diameter are more severely modified leading to the formation of a central uplift and concentric rings and terraces (complex crater) (e.g., French 1998; Koeberl 2014).

Following the common nomenclature, impact rocks (which are all rocks created or modified by hypervelocity impacts) can be classified into proximal and distal impact ejecta according to their distance from the impact site: impact ejecta transported less than 2.5 crater diameters are called proximal ejecta, whereas those deposited at greater distances are called distal ejecta. (e.g., Stöffler and Grieve, 2007). The former comprise shocked rocks, impact melt rocks as well as monomict and polymict impact breccias with (suevite) or without (lithic breccia) melt particles (e.g., Stöffler and Grieve, 2007). Contrary, distal impact ejecta can be classified into tektites, microtektites and air fall beds. While Tektites are millimeter to centimeter sized and deposited on land, microtektites are typically smaller than one millimeter and found in deep sea sediments (e.g., Koeberl, 2014 and references therein). Both can exhibit various rotational shapes, such as dumbbells, discs, pears, and teardrops, but for microtektites spheres are most common (e.g., Glass, 1967; Glass and Simonson 2012). Ejecta found more than ~10 crater diameters away from large impact craters consist primarily of glassy spherules. Such spherules (including those from the Barberton area) are droplets solidified from melt or condensed from vapor inside a so-called impact vapor plume (e.g., Johnson and Melosh, 2012; Glass and Simonson 2012; Goderis et al. 2013, Koeberl 2014). If they consist of pure glass they are termed microtektites, whereas they are called microkrystites if they contain primary crystallites, such as Ni-rich Cr-spinels (e.g., Goderis et al. 2013). Figure 2 visualizes the basic nomenclature of all kinds of impactites.

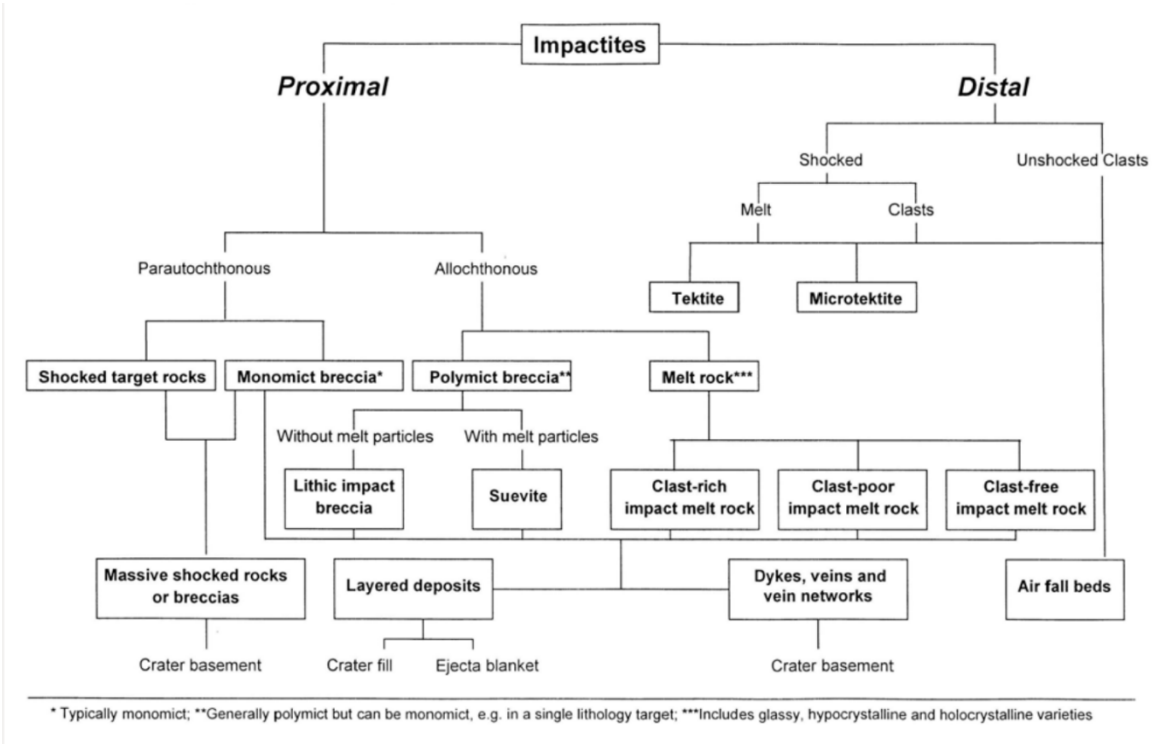

Figure 2. *Classification scheme of impactites (after Stöffler and Grieve, 2007).*

1.3 Study area

The Kaapval Craton in South Africa is composed of five Greenstone Belts separated by tonalite-trondhejmite-granodiorite batholites of which the Barberton Greenstone Belt (BGB) is the largest (e.g., Lowe and Byerly, 1999, 2007; Anhaeusser, 2014). Lithostratigraphically the BGB is divided into three Groups (Onverwacht Group, Fig Tree Group and Moodies Group), which together form the 3.2-3.5 Ga old Swaziland Supergroup. The Onverwacht Group has a thickness of ~15 km and formed between 3.55 and 3.30 Ga (e.g., Anhaeusser, 2014). It is dominated by ultrabasic to basic volcanic rocks like komatiites and basalts with minor occurrences of felsic volcanic rocks and sedimentary rocks (Lowe and Byerly, 1999; Anhaeusser, 2014). The predominantly sedimentary Fig Tree Group, overlying the Onverwacht Group, formed between 3.260 to 3.226 Ga and was deposited in a variety of sedimentary environments ranging from deep to shallow water and alluvial to fan delta (e.g., Lowe and Byerly, 2007; Anhaeusser, 2014). The Inyoka fault separates the Fig Tree Group into a northern and a southern part. In the northern part five formations have been distinguished composed of shales, cherts, turbiditic sandstones, and schists, while in the southern part of the Inyoka fault two formations exist, made up of conglomerates, shales, volcaniclastic rocks, breccias, and sandstones (e.g., Anhaeusser, 2014). The uppermost Moodies Group contains three formations of fining upward clastic sediment

sequences and banded iron formations, which were deposited ~3.23 Ga ago (e.g., Heubeck et al. 2013; Anhaeusser, 2014). The rocks of BGB are mostly of low metamorphic grade and were intruded by a variety of granitoids along its margins during several episodes between 3.50 and 3.20 Ga (e.g., Anhaeusser 2014).

According to Glass and Simonson (2012), seven spherule layers (S1 to S7) have been found in Onverwacht Group and Fig Tree Group since the late 1980s. The spherules are mostly spherical and secondary alteration has often completely obscured their original mineralogy. They usually occur in cm-thick beds intercalating shale or chert, some showing evidence of tsunami events associated with the impact (e.g., Lowe et al. 2003). However, the impact origin of BGB spherule layers has long been doubted, mainly because of extremely high concentrations of HSE associated with sulfides, which have been interpreted as products of secondary alteration (e.g., Koeberl et al., 1993; Koeberl and Reimold, 1994, 1995). Meteoritic admixtures in impactites rarely exceed 1%, with a few cases of up to 10 % (e.g., French and Koeberl, 2010; Koeberl, 2014), whereas some of the BGB layers exhibit superchondritic HSE concentrations (Johnson et al., 1999). Finally, ^{54}Cr isotope signatures provided an unambiguous evidence for the impact origin for some of the layers (Kyte et al., 2003; Mougel et al., 2017). However, the causes and mechanisms for the extreme HSE enrichment in the Archean spherule layer are still not well understood.

Up to 25 new spherule layers have been discovered in two recently drilled cores in the Barberton area: the 763 m long BARB5 core, recovered during the International Scientific Drilling Program (ICDP) project in the Barite Valley Syncline in the central BGB, and the CT3 core, drilled by an exploration company (Sabi Gold) in the northeastern BGB (Mohr-Westheide et al., 2015; Fritz et al., 2016; Ozdemir et al., 2016).

The sample used for this study was derived from the BARB5 core. It was drilled into the lower Mapepe Formation of the Fig Tree Group and contains eight spherule bearing intervals (A to H) between 512.6 and 510.5 m depth (Fritz et al., 2016). The confirmation of the impact origin of some of the BARB5 spherule layers was currently undertaken by Schulz et al. (2017) on the basis of siderophile element systematics, as well as $^{187}Os/^{188}Os$ isotope signatures (see discussion below). For this study a sample from a BARB5 spherule layer was selected with an approximated meteoritic admixture of ~80% (Schulz et al., 2017). However, Schulz et al. (2017) analyzed spherule-

groundmass (spherule-shale) aggregates, leaving the question in which of the two lithologies (spherules or matrix) the projectile component is hosted or if it is partitioned in equal proportions between both. In chapter 5 the approach undertaken in this study is outlined to answer this question. However, it might be useful to take a closer look at the basic tools currently utilized to identify meteoritic admixtures within impactites.

1.4 The geochemistry of impactites

Not every circular depression on the Earth`s surface is of impact origin. Endogenic forces (e.g., volcanism; tectonism) are capable of producing structures that might (more or less) closely resemble the typical appearance of an impact crater. Four types of evidence are typically utilized in order to confirm the extraterrestrial nature of such structures and which are uniquely related to hypervelocity impacts events. These are (i) preserved meteoritic fragments, (ii) shatter cones, (iii) shocked minerals, and (iv) chemical and isotopic projectile signatures (for a recent review see Koeberl, 2014). Meteoritic fragments are extremely rare as most meteorites melt or evaporate completely during the impact (e.g., French and Koeberl 2010). Shatter cones are the only megascopic evidence visible in hand-specimen to outcrop scale (e.g., Dietz, 1968). They appear as distinctive multiple sets of striated conical fractures that can form in large volumes of target rocks of all kinds (Dietz, 1959, 1963a, b, 1968; Milton, 1977; Koeberl, 2014). Irreversible high-pressure shock-wave effects on minerals include planar microdeformation features (planar fractures, planar deformation features: PDFs), optical mosaicism, changes in refractive indices, birefringence and optical axis angle, isotropization (e.g., formation of diaplectic glasses), phase changes, and kink bands (for a summary see Koeberl, 2014 and references therein).

This chapter focuses on the geochemical tools suited for the identification of meteoritic admixtures within impactites. Such extraterrestrial fingerprints are imprinted to the target rocks during recondensation events (of the vaporized projectile) and/or melting events.

The tools to identify projectile materials all make use of differences (either geochemically or isotopically) between the projectile material (e.g., chondrites or iron meteorites) and the typical target material (upper continental crust; UCC). Only few elements and isotopes fulfill this requirement, such as the moderately siderophile elements (Cr, Ni, and Co) and the HSE (e.g., Re, Os, Ir, Pt), or (for example) the isotopes ^{187}Os and ^{54}Cr.

Because of the depletion in siderophile elements of the UCC in comparison to undifferentiated meteorites (chondrites) or, even more pronounced, iron meteorites (Kong et al., 1996), this element group is ideally suited to detect projectile admixtures to target rocks. Even small admixtures of meteoric components are, thus, detectable in impact related rocks that incorporated vaporized projectile material. Geochemical tools for the identification of meteoritic admixtures to target rocks have successfully been used for ~40 impact structures and also for Archean spherule layers (e.g., Koeberl, 2014).

1.4.1 Moderately siderophile elements

Chromium, Ni, and Co and their corresponding interelement ratios are often used for suggesting the possible presence of extra-terrestrial material (e.g., Palme et al. 1978; French and Koeberl, 2010). Unfortunately, the differences in concentrations of these elements between crustal rocks and meteorites are often low and elevated concentrations may be derived from the target rocks. If sensitive enough (in case of a highly silicic target), interelement ratios of Cr, Ni and Co concentrations in impactites could, in principle also provide clues about the type of impactor (e.g., Palme et al., 1978; Evans et al., 1993).

1.4.2 Highly siderophile elements

Highly siderophile elements, e.g., the platinum group elements (PGE) (Os, Ir, Pt, Ru, and Pd) and Re, are more suitable for the identification of meteoritic components in impactites compared to the moderately siderophile elements, as their abundance differences between meteorites (excluding achondrites, which are, however, a rare type of projectile material on Earth) and the UCC are even more pronounced (see Fig. 3). However, enrichments and near chondritic interelement ratios of these elements do not always point towards impact origin but could also be caused by contamination with basic or ultrabasic rocks from the mantle, such as komatiites (see discussion in Schulz et al.,

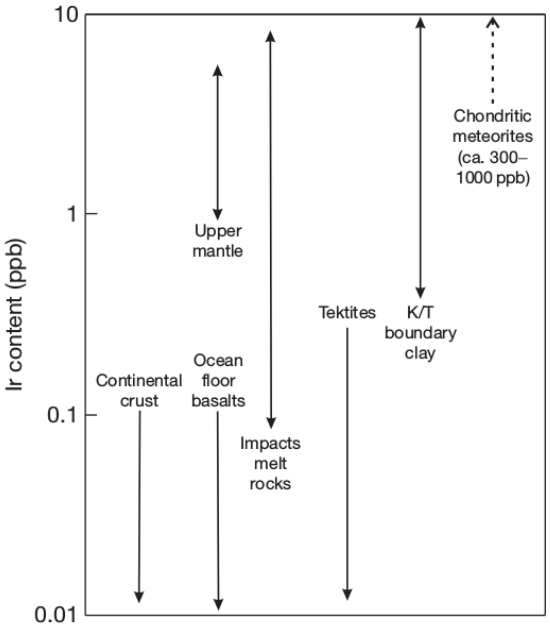

Figure 3. *Range of Iridium contents in various terrestrial materials compared to chondrites. All other HSE (except Re) follow a similar trend (from Koeberl, 1998).*

2016). Therefore, careful petrographic and isotopic studies are required to exclude any such mafic or ultramafic target contributions (which can simulate a meteoritic component).

1.4.3 The ^{187}Re- ^{187}Os isotopic system

The ^{187}Os/^{188}Os and ^{187}Re/^{188}Os ratios are used for the identification of meteoritic admixtures. Due to the, compared to the UCC, extremely high Os abundances in chondrites and iron meteorites (see discussion above and Fig. 3) and their unradiogenic ^{187}Os budgets, even very small additions of meteoritic matter lead to a characteristic ^{187}Os signature in the impactites. The UCC typically exhibits ^{187}Os/^{188}Os ratios of ~1.40 (Peucker-Ehrenbrink, 2001), whereas chondrites exhibit values ranging from 0.1254 to 0.1305 (e.g., Tagle and Berlin, 2008). However, chondrites and the Earth's mantle have almost identical ^{187}Os/^{188}Os values of around 0.13 (e.g., Meisel et al., 2001). This leads to similar complications during the projectile identification as explained above, making careful petrographic studies necessary. Figures 4a and 4b show the typical mixing relationships between target materials from the impact site and projectile materials in the ^{187}Os/^{188}Os vs. Os (Fig. 4a) and ^{187}Os/^{188}Os vs. ^{187}Re/^{188}Os diagrams (Fig. 4b). It should be noted that Schulz et al. (2017), as already mentioned above, applied this method to some of the BARB5 spherule layers, confirming their impact nature and admixtures of projectile components of up to 100%.

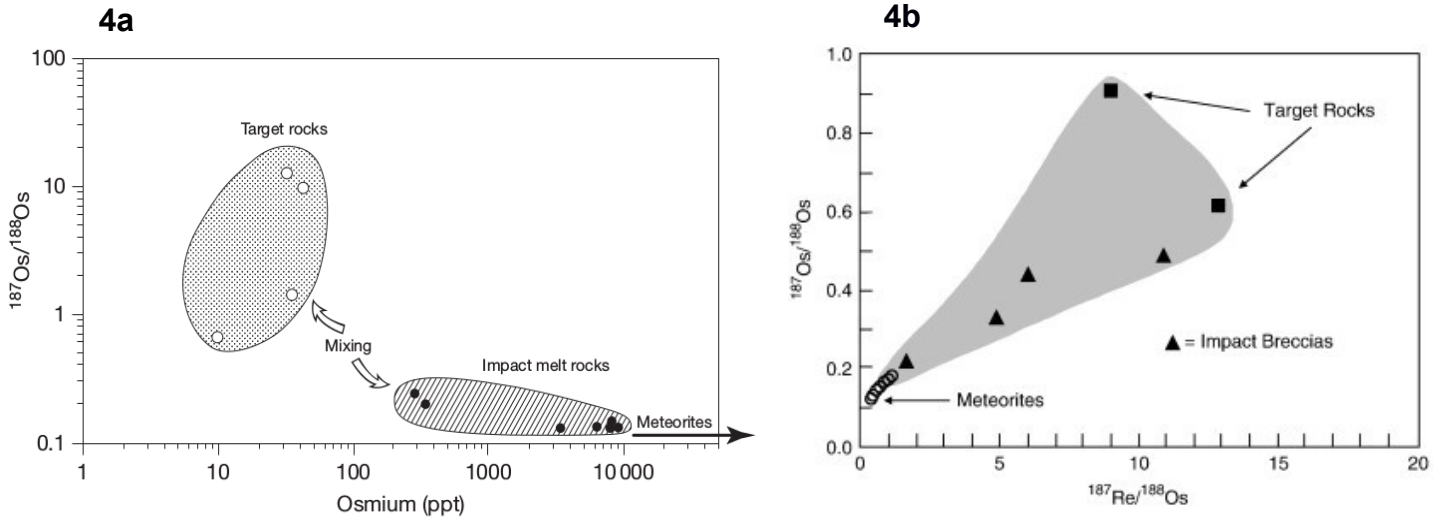

***Figure 4a** and **4b** ^{187}Os isotopic ratios vs. Os content and Re-Os isotopic diagram used as mixing diagrams between meteorites and target rocks. Impactites plot between the two endmembers (from Koeberl, 2014).*

1.4.4 Chromium isotopes

The chromium isotopic system is another tool suited to detect meteoritic admixtures in impactites (e.g., Mougel et al. 2017). This tool is based on the radioactive decay of the extinct radionuclide ^{53}Mn to ^{53}Cr with a half-life time on 3.7 Ma and the heterogenic distribution of ^{54}Cr in various meteorite types (e.g., Shukolyukov and Lugmair,1998). ^{53}Cr/^{54}Cr and ^{52}Cr/^{54}Cr isotope ratios can be used to characterize the type of impactor and identify extraterrestrial admixtures due to significant nucleosynthetic anomalies of ^{54}Cr between various extraterrestrial materials and the Earth.

As mentioned earlier, this system was also used to unambiguously confirm the impact genesis of the spherule layers from the Barberton area, terminating decade long discussions on the hydrothermal origin of the elemental signatures observed within the layers. Kyte et al. (2003) reported the presence of carbonaceous chondrite-like material with up to 60 % to some of the S2 to S4 spherule layers, albeit with strong inter-layer variations.

2. Samples and analytical methods

2.1 Samples

The sample used for this study was derived from the core interval between 511.29 and 511.51 m depth of the recent International Continental Scientific Drilling Program (ICDP) drill core BARB5 from the Barberton Mountain Land (South Africa). This interval contains, inter alia, four ~4 cm thick spherule layers (labelled B to E) consisting of densely packed, 0.3-2 mm sized spherules separated by up to 1.5 cm thick carbonaceous shale bands (termed intercalations; IC) (Mohr-Westheide et al., 2015; Fritz et al., 2016; Schulz et al. 2017). Mineralogically, the spherule layers consist of quartz–phyllosilicate–K-feldspar–Mg siderite–barite–calcite assemblages (Mohr-Westheide et al., 2015). The whole core section was cut into 22 subsamples and labeled according to Fig. 5. The spherule-groundmass assemblages (spherule-shale or nearly spherule free intercalations) were analyzed by Schulz et al. (2017) and layer B and layer C to E were postulated to have formed by (at least) two separate impact events (layers C to E, probably representing a single impact event, might have been duplicated by sedimentary processes; Fritz et al., 2016; Schulz et al., 2017). Whereas layer B, according to the siderophile element budgets and ^{187}Os isotopes, exhibits, depending on the type of chondrite, maximum meteoritic admixtures of up to ~9 %, layers C to E were shown to contain up to ~40-100% of a chondritic component (Schulz

et al., 2017) (see Fig. A1). Furthermore Ni-rich chromium-spinels were observed in some of the layers (within and outside the spherules embedded in the shaly groundmass) and these are suspected carrier phases of the meteoritic component (Mohr-Westheide et al., 2015).

For this study a ~200 mg sub-sample from spherule layer E (core depth 511.25 m) was selected for spherule extraction. This sample was chosen because it contains a high meteoritic component and because of the undeformed nature of this layer (Fritz et al., 2016).

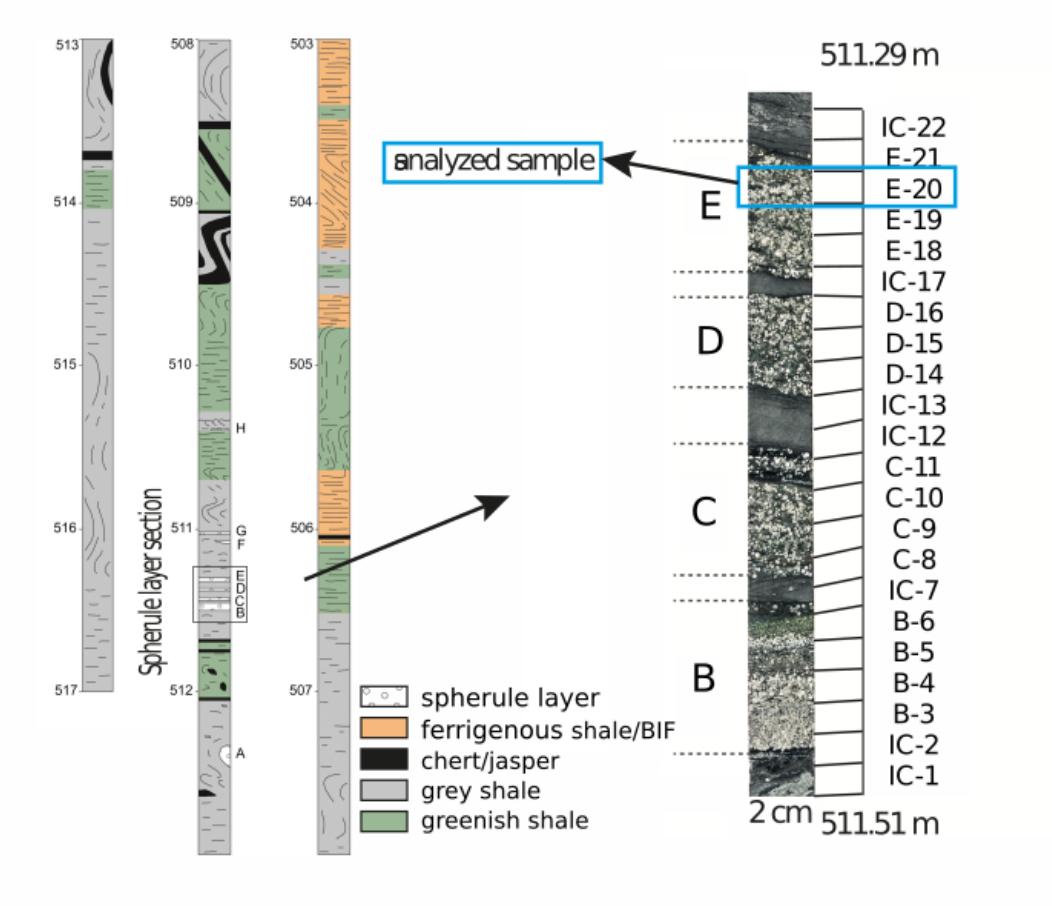

Figure 5. *Stratigraphic column of the BARB5 drill core from 517 to 503 m through the spherule-bearing core interval (left) and cross section of the spherule layer section (511.51 to 511.29 m), showing the B-E spherule layers in the BARB5 drill core (right). Numbers refer to depth in meters in the core. Layer E-20, analyzed in this study, is highlighted (blue rectangle) (modified from Fritz et al., 2016; Schulz et al., 2017).*

2.2 Sample preparation and analytical methods

2.2.1 Sample preparation (hand picking)

As first step of sample preparation the sample (E-20) from the BARB5 spherule layer section was cleaned in an ultrasonic bath in 1 M HCl for 20 min (all 22 samples splits were cut from the drill core section, not as a part of this study, using a diamond wire saw at the Natural History Museum Berlin in 2015). After gently crushing the sample in an agate mortar into various grain size fractions (to achieve optimal spherule separation), pure spherule and groundmass (carbonaceous shale) separates were obtained via handpicking under a binocular. Due to the small size and often unregular shapes of the spherules (dumbbell, ovoid, or broken) no perfect separation of spherules from groundmass was achieved. Instead, a highly spherule-enriched separate (> ~95% spherules) and a highly spherule-depleted groundmass separate (< ~5% spherules) were obtained. These separates are termed “spherule sample“ and “matrix separate“ throughout this study. The mixed separate (called “mix“) comprises remixed not separable components and not a representative bulk of sample E-20. In this study, 81.73 mg spherule sample, 53.86 mg matrix separate, and 53.57 mg sample powder of the unseparated mix, were obtained.

A basic outline of the wet chemical and analytical procedures applied in this study is schematically shown in Fig. 6. Sample preparation and high pressure asher (HPA) treatment was the same for all samples. After solvent extraction, the wet chemical procedure continues in two directions (see Fig. 6). One of them dedicated for Os extraction, purification and measurement of Os concentrations (via isotope dilution, see chapter 2.3) as well as ^{187}Os isotope composition via negative thermal ionization mass spectrometry (N-TIMS) and one of them dedicated for Re, Ir, and Pt extraction via anion exchange chemistry and concentration determination via inductively coupled plasma mass spectrometry (ICP-MS). All steps are explained in detail below.

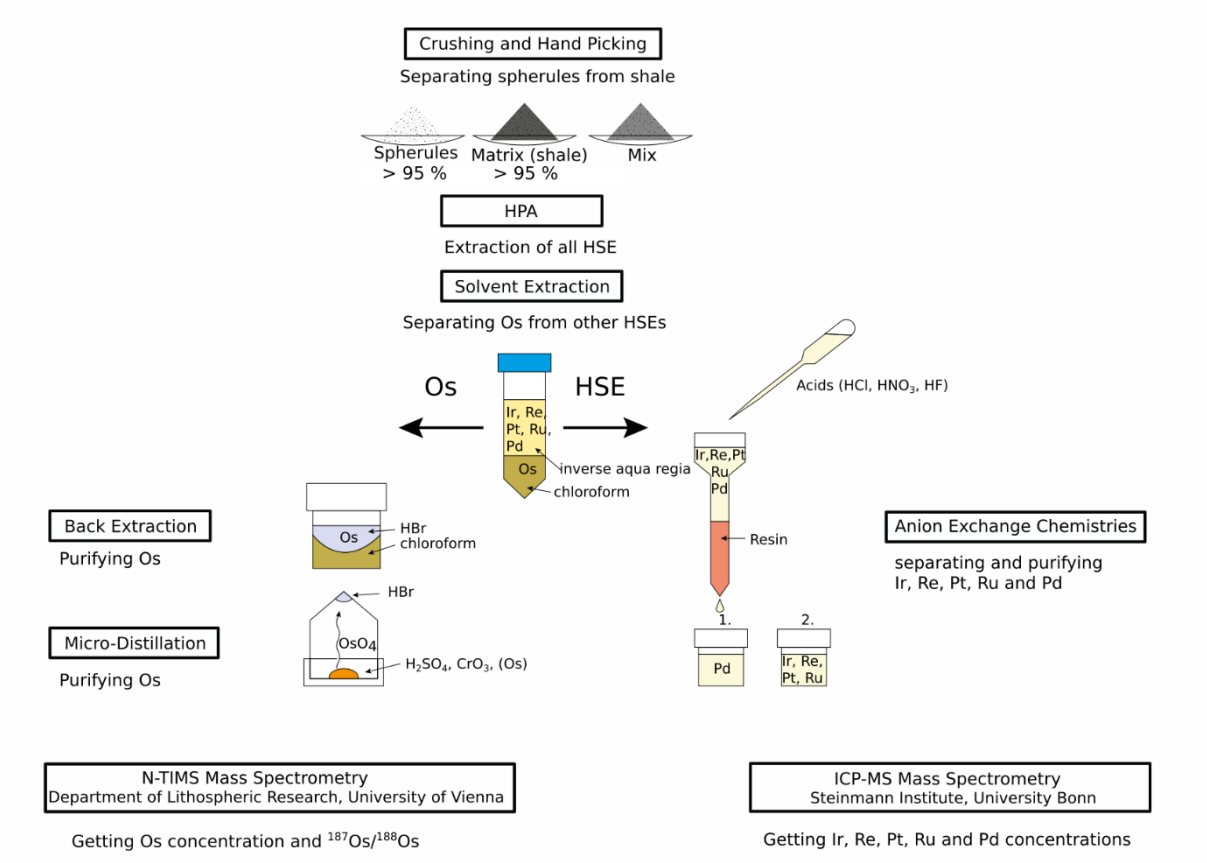

Figure 6. *Workflow scheme outlining and sketching all steps of sample preparation and analytical methods applied in this study.*

2.2.2 High pressure asher dissolution (extraction of HSEs)

Prior to high pressure asher dissolution the dry sample powders were spiked with a mixed tracer enriched in ^{185}Re,^{190}Os,^{191}Ir, and ^{194}Pt isotopes (see chapter 3.3). The spiked separates were digested in 5 ml inverse aqua regia (HNO_3 + HCl: 3 ml + 2 ml) and treated over night at 270 °C and between 100-130 bar in an Anton Paar high pressure asher (HPA) to achieve sample-spike equilibration. During this process, virtually all HSEs were leached into the acid mixture (except Re, which only partly partitions into the aqua regia; see discussion below).

2.2.3 Solvent extraction (separating Os from all the other HSEs)

Solvent extraction follows the general procedure as described by Cohen and Waters (1996). It is applied to separate Os from all the other HSEs and takes advantage of the high affinity of Os to organic phases (in this case chloroform). The cooled down glass vials were opened and after adding about 4 ml chloroform, immediately sealed with Parafilm to prevent any loss of volatile OsO_4. All the liquid, but not the undissolved sample sediment, was transferred into a 50 ml centrifuge tube. Two ml chloroform were added and each sample solution was mixed on a sample-

mixer for about 10 min before removing the organic phase (containing the Os) with a pipette to a 15 ml Savillex beaker (prefilled with 4 ml hydrobromic acid). This step was repeated three times to extract all Os. All Savillex beakers (now containing a chloroform-HBr mix) were mixed over night on the sample-mixer.

The remaining aqua-regia and the sediment from the glass vials containing the other PGEs and Re was transferred to another set of 15 ml Savillex beaker and dried down on a hotplate at 110 °C overnight.

2.2.4 Back extraction and micro-distillation (purifying Os)

Back extraction is a purification step during which Os moves from the organic phase (chloroform) into HBr with the aim to stabilize Os in solution (as a hexabromo complex). This technique is described in detail in Cohen and Waters (1996). The separation of chloroform from the HBr (containing the Os) was performed using micro-pipettes. The HBr was then dried down on a hotplate at only 70 °C over two days to avoid loss of volatile Os.

Even though very low concentrations of other elements are coextracted with the Osmium during the solvent and back extraction procedures, the micro-distillation technique (after Roy-Barmann and Allegre, 1995) was performed as a final step of Os-purification. During this step Os evaporates from 10 µl of sulfuric acid (into which the Os cut was redissolved after drying down the HBr) at 90°C for two hours, using a strong oxidizing agent (Cr(VI) solution), and then partitions into a 10 µl HBr-spot in the tip of a sealed upside-down rocket beaker (see Fig. 6 for a visualization). Before N-TIMS measuring, this HBr-spot containing all OsO_4 is dried down to about 3 µl table top on a hotplate at 90 °C.

2.2.5 Anion exchange chemistry (separating and purifying HSEs)

While all the other elements are leached during HPA treatment, some of the Re remains in the sediment. Thus, the PGE cut is dried down and redissolved several times to dissolve silicates and metals: first in 4 ml concentrated HF and trace HCl in closed Teflon beakers at 120°C overnight, then in 4 ml concentrated HNO_3 and finally in 4 ml concentrated HCl to convert the sample to chloride form.

The HSE separation was then performed using an anion exchange technique with 10 ml columns containing 1 ml AG1x8-resin. This was done following a procedure adapted from the method of Chu et al. (2014) by using 6 M HNO_3, concentrated HNO_3, 1 M and

concentrated HCl as eluents in a first step, and then by using 2 M HF, 1 M HF, 6 M HCl, and concentrated HCl in a second, so called clean-up, step. Between the two steps the cuts are dried down and redissolved in 1 M HCl (both recipes are given in the appendix).

2.3 Mass spectrometry

Mass spectrometers ionize the sample and then sort nuclides by their charge to mass ratio in a magnetic field, where they are deflected in varyingly excentric curvatures. In the ion source of the mass spectrometer the sample is vaporized and a beam of charged particles produced, which is then separated into its components in the magnetic field of the analyzer and counted in the collector (e.g., Vogl and Pritzkow, 2010; Encyclopædia Britannica, 2017). There are various types of ion sources in mass spectrometers. Thermal ionization and inductively coupled plasma are used in this study. To amplify the signal, a secondary electron multiplier (multiple sets of dynodes exponentiating the number of ions) are used. In this so called single-collector mode the ion beam of every isotope is measured step-wise for only a few seconds (peak jumping mode).

During mass spectrometric analyses, two complications have to be accounted for, mass interference and mass fractionation:

Nuclides with the same mass to charge ratio cannot be distinguished (e.g., ^{187}Re and ^{187}Os). This effect is called mass interference and can be accounted for by measuring simultaneously (to all other isotopes of interest) an interference-free isotope of the same element which causes the interference (in the case of the ^{187}Re-^{187}Os example one also measures ^{185}Re, which is interference-free, and occurs in natural -terrestrial- samples in a known ratio to ^{187}Re, allowing to subtract the contribution of ^{187}Re from the signal intensity on mass 187).

The fact that lighter nuclides preferentially evaporate from a reservoir during heating is called mass fractionation. This effect continuously changes the isotope ratio during the course of a measurement. This effect can be accounted for by applying several mathematical procedures (called linear or exponential mass fractionation law) which make use of the exact isotope masses and the measured isotope ratios during the course of the measurement as input parameters.

In this study, HSE concentrations (Re, Os, Ir, Pt) were measured using isotope dilution mass spectrometry. Isotope dilution mass spectrometry is a technique for high precision element concentration measurements. The isotopic composition of the analyte is known and its mass is to be ascertained. Therefore, a known amount of a so-called spike of known isotopic composition, usually enriched in the rarest natural isotope of the analyte, is added to the sample. After equilibration and measuring the isotopic composition of the sample-spike-mixture via mass spectrometry, the concentration of the element of interest can be calculated (see Appendix). The main advantage of this technique is that element separation does not have to be quantitative as soon as sample and spike are equilibrated (e.g., Botha, 2010).

2.3.1 Negative thermal ionization mass spectrometry

Osmium isotope ratio measurements and Os concentration measurements were carried out at the Department of Lithospheric Research at the University of Vienna using a Thermo Finnigan Triton Thermal Ionization Mass Spectrometer operating in negative mode. Together with a saturated solution of $NaOH/Ba(OH)_2$ as an activator (Völkening et al., 1991; Creaser et al., 1991) Os was loaded as a bromide on a single Pt ribbon filament. Osmium was then measured as OsO_3^- ions using the Triton SEM detector in a peak hopping measurement sequence. Isobaric interferences attributable to W- or Pt-oxide were not observed. Isobaric interferences of ^{187}Re on ^{187}Os were monitored by measuring $^{185}ReO_3^-$ (mass 233) and were corrected if observed. Mass fractionation was corrected offline using $^{192}Os/^{188}Os = 3.083$ (Brandon et al., 2005; Luguet et al., 2008). As oxygen occurs as ^{16}O, ^{17}O, and ^{18}O, oxygen correction has to be performed using $^{17}O/^{16}O$ of 0.0003866 and $^{18}O/^{16}O$ of 0.00203406 (see van Acken et al., 2011 and references therein).

The best temperatures to measure Os typically are between 720 and 780°C, achieved via step-wise heating until a sufficiently large signal intensity is reached (typically 100.000 counts on ^{192}Os, or, depending on the sample/spike ratio, at 200.000 counts on ^{190}Os). Due to their elevated Os concentrations (compared to typical upper continental crust rocks) all separates from this study were measured between ~700 and ~750°C at, mostly, around 500.000 counts. It should be noted, however, that all samples were spiked in an optimal range ($^{190}Os/^{192}Os$ between 1 and 5), allowing for precise (<3% 2σ RSD) Os concentration determinations. During the course of the

sample measurements a DROsS (Durham Romil Osmium Standard) solution was measured to check for unusual mass fractionation effects. The typical isotope ratios for all osmium isotopes were measured (e.g., 0.1609 for $^{187}Os/^{188}Os$; e.g., Luguet et al., 2008). The blank for Os was 2± 1 ppt.

2.3.2 Inductively coupled plasma mass spectrometry

Rhenium, Ir and Pt contents were measured using a Thermo Element XR SF-ICP-MS in single collector mode at the Steinmann-Institute at the University of Bonn, Germany, using methods described in Luguet et al. (2015). The oxide rate (to correct for mass interferences) was continuously monitored throughout the measurements. Total blanks (n=4) were ~4 pg for Re, ~3 pg for Ir and ~22 pg for Pt. Due to the extremely high concentrations of HSE in most of the analyzed samples, blank corrections were negligible in all cases.

For quantification of precision and accuracy of the HSE chemistry and analytical procedures, replicate analysis were performed on international reference materials. The references were chosen to cover a wide range of concentrations: TDB-1 (diorite, CANMET, international standard material; see Ishikawa et al. 2014 for details) with Re, Os and Ir concentrations < 100 ppt, and OKUM (komatiite, IAG-certified ultramafic rock reference material; Burnham et al. 2010 and Meisel et al. 2013) with Os and Ir concentrations of ~ 1000 ppt. Within 2σ uncertainty, averages and relative standard variations of element concentrations of all measured HSE for these two reference materials were in excellent agreement with the literature data.

***Table 1**. Concentrations (in ppb) of Re, Os Ir, and Pt, Os/Ir ratios, and $^{187}Os/^{188}Os$, $^{187}Re/^{188}Os$, and initial $^{187}Os/^{188}Os$ isotope ratios, the latter back-calculated to the age of middle Mapepe formation (3.32 Ga; Lowe and Byerly, 1999), measured in this study for separates from layer E of the BARB5 spherule layer, as well as data for other BARB5 spherule layers, Fig Tree Group sediments, and chondrites. Data from this sample are in bold.*

	Re	Os	Ir	Pt	Os/Ir	$^{187}Os/^{188}Os$	±2σ	$^{187}Re/^{188}Os$	±2σ	$(^{187}Os/^{188}Os)_i$	±2σ
Matrix separate	**3.696**	**171.2**	**205.5**	**5950**	**0.833**	**0.1077**	**0.00017**	**0.1025**	**0.0031**	**0.1018**	**0.0031**
Spherule sample	**2.296**	**83.78**	**70.29**	**185.0**	**1.192**	**0.1058**	**0.00029**	**0.1301**	**0.0039**	**0.1058**	**0.0032**
Mix	**18.14**	**104.9**	**107.5**	**258.6**	**0.976**	**0.1060**	**0.00007**	**0.8206**	**0.0246**	**0.05932**	**0.0018**
BARB5 layers B-E *	0.04-26.1	1.46-944.5	4.53-552	5.22-2082	0.218-3.775	0.1064-0.3161		0.0101-0.1464		0.1054-0.2217	
Fig Tree Group Sediments °		0.05-0.792	0.153-0.651	1.03-3.81	1.02-1.40	0.3744-0.7864					
Chondrites [x]		364-2850	336-2635	707-1596	1.05-1.13	0.12543-0.13045		0.3731-0.4779		~0.1048	

*[x] Shirey and Walker 1998; ° Siebert et al., 2005; Tagle and Berlin, 2008; *Schulz et al., 2017*

3. Results

3.1 Geochemistry

Highly siderophile element (Re, Os, Ir, Pt) concentrations and Os/Ir interelement ratios for samples analyzed in this study as well as the range of values for bulk samples of the BARB5 spherule layer section, Fig Tree Group sediments (graywackes, metapelites, siltstones, and black shales from various locations in BGB; see Siebert et al., 2005 for exact locations and description), and chondrites (range of ordinary, carbonaceous and enstatite chondrites) are given in Table 1. The Fig Tree Group sediments represent the target lithology unaffected from the impact, while chondrites are the supposed impactors. The spherule layers are presumably formed by mixing of these two components.

Rhenium concentrations range from 2.296 (spherule sample) to 18.14 ppb (mix) with the matrix separate (nearly spherule-free shale sample) exhibiting 3.696 ppb and are comparable to the range measured for bulk BARB5 spherule samples (spherule-groundmass assemblages) from the spherule layer section measured by Schulz et al. (2017), which range from 0.04 to 26.1 pbb.

Platinum group element concentrations of the separates show variations from 83.73 to 171.2 ppb for Os, 70.29 to 205.5 ppb for Ir and 185.0 to 595.0 ppb for Pt with the matrix separate exhibiting the highest concentration, the spherule enriched sample exhibits the lowest concentrations and the contents in the mixed sample are between those of the two separates (104.9 ppb Os, 107.5 ppb Ir, and 258.6 ppb Pt).

All these HSE concentrations are comparable to spherule-groundmass assemblages (bulk samples) of BARB5 spherule layer sections analyzed by Schulz et al. (2017) e.g., <300 ppb for Os and 139 ppb for Ir in layer E (same subsample as this study). Average Fig Tree Group sediments all exhibit HSE concentrations up to three orders of magnitude lower compared to the samples analyzed in this study (Siebert et al., 2005).

3.2 Rhenium-osmium isotope systematics

Present day (measured) $^{187}Os/^{188}Os$ isotope ratios as well as $^{187}Os/^{188}Os$ isotope ratios back-calculated to the age of the middle Mapepe Formation of the Fig Tree Group (i.e. 3.32 Ga; Lowe and Byerly, 1999) are given in Table 1. The measured $^{187}Os/^{188}Os$ isotope ratios of the three samples analyzed in this study are all very similar and range from 0.1058 ± 0.00029 (spherule sample) to 0.1077 ± 0.00017 (matrix separate), with

the mixed sample being in between (0.1060 ± 0.00007). Notably, these values are all subchondritic (chondrites range from 0.12543 to 0.13045; Shirey and Walker, 1998) and are less radiogenic than most present-day $^{187}Os/^{188}Os$ ratios reported for spherule-groundmass assemblages and intercalations from the spherule layer sections of the BARB5 core (ranging from 0.1064 to 0.3161; Schulz et al., 2017). Non-impact related Fig Tree group sediments range from 0.3744 to 0.7864 (Siebert et al., 2005). The only lithology in the Barberton Greenstone Belt with comparably low $^{187}Os/^{188}Os$ isotope ratios are volcanic rocks, such as komatiites, ranging from ~0.1048 to ~0.1970 (Puchtel et al., 2009, 2014; Connolly et al., 2011).

Back-calculated (to an age of 3.32 Ga) $^{187}Os/^{188}Os$ ratios range from 0.05932 ± 0.0018 for the mix to 0.1018 ± 0.0031 for the matrix separate and 0.1058 ± 0.0032 for the spherule sample and count among the lowest values measured for BARB5 samples so far. Initial $^{187}Os/^{188}Os$ ratios from the BARB5 core, analyzed by Schulz et al. (2017), range from 0.1030 to 0.2764.

The $^{187}Re/^{188}Os$ isotope ratios of samples analyzed in this study range from 0.1025 ± 0.0031 for the matrix separate to 0.1301 ± 0.0039 for the spherule sample and 0.8206 ± 0.0246 for the mixed sample. The mixed sample is out of the range of spherule layer samples of BARB5 (~0.01 to ~0.31; Schulz et al., 2017) but within the range of typical sediments of the Fig Tree Group exhibiting values from ~0.4 to ~9 (Siebert et al., 2005).

4. Discussion and conclusions

4.1 Spatial distribution of the carrier phase

Preliminary studies revealed that significant meteoritic admixtures have been found in spherule-matrix assemblages and in spherule-free intercalations, suggesting that the meteoritic component is not strictly related to (or sited within) the spherules (Schulz et al. 2017). The highest meteoritic admixtures in the BARB5 spherule layer section, indicated by the highest HSE concentration (of up to 944.5 ppb Os) and the lowest $^{187}Os/^{188}Os$ isotope ratio (0.1064 ± 0.0001), were found in a spherule sample from layer C. However, several (nearly spherule-free) intercalations exhibit similarly high HSE contents (Fig. 7).

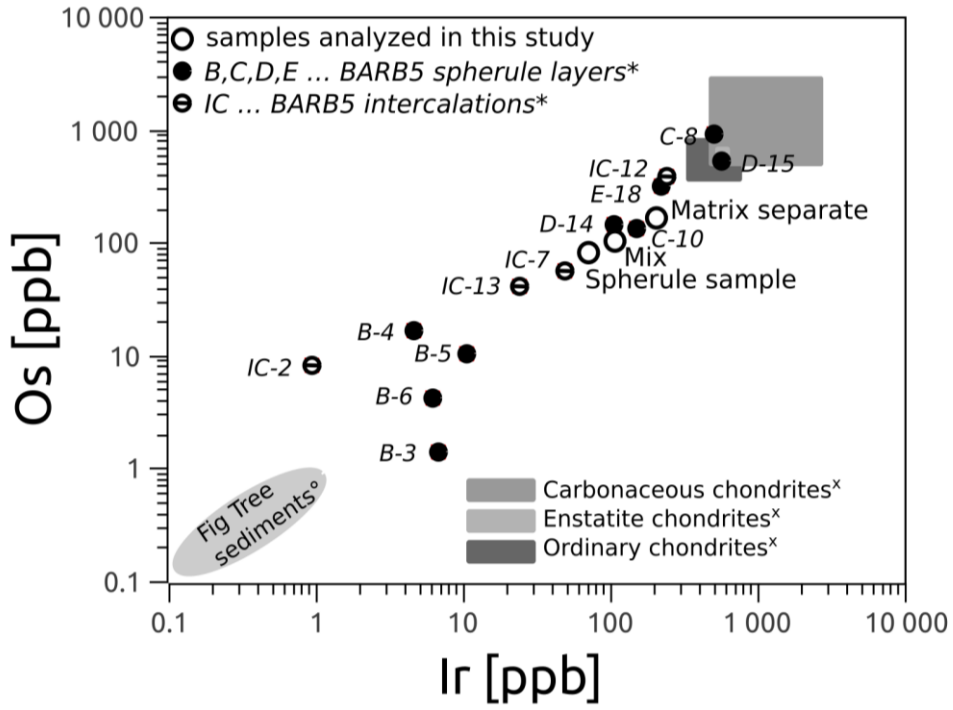

Figure 7. *Osmium vs. Ir abundance plot for samples of this study and for BARB5 spherule layer section compared to Fig Tree Group sediments, and chondrites. All samples plot along the mixing line between chondrites and Fig Tree Group Sediments (i.e., crustal target rocks). (° Siebert et al., 2005; ˣ Tagle and Berlin, 2008; * Schulz et al., 2017)*

These observations invoke the question, whether or not there is any meteoritic component in the spherules, as the higher meteoritic admixtures in the spherule-matrix assemblages measured by Schulz et al. (2017) could be the result of high concentrations of meteoritic carrier phase(s) in the matrix. However, petrographic studies and detailed element mapping, undertaken by Mohr-Westheide et al. (2015), provided evidence for the frequent occurrence of Ni-rich Cr-spinels (suspected primary constituents and carrier phases of the projectile component) in spherule layers of the BARB5 drill core section and these are hosted within and outside the spherules. Furthermore, alteration has effected the distribution of the PGEs (meteoritic carrier phase). Mohr-Westheide et al. (2015) reported the occurrence of grains of PGE alloys only within unaltered spinels without a rim, and PGE sulfarsenides, the product of secondary hydrothermal or metamorphic overprint, in the matrix near altered spinel (see Fig. 8). Hence, the PGEs were transport, but only over very limited (µm) scale. A rough calculation on the base of Pt shows, that it would need ~8.56 to ~3470 ppb PGE alloy get the measured Pt contents of the BARB5 spherule layers (see Appendix). This is a reasonable result, supporting the hypothesis that Ni-rich Cr-spinel-related PGE phases are the long sought meteoritic carrier phase.

Due to primary heterogenous fallout the PGEs cluster and cause nugget effects, accounting for the big differences between the spherule layers, and even within different subsamples of one layer (Mohr-Westheide et al., 2015; see Fig. 7). Also, Fritz et al. (2016) reported size-dependent differential settling of various particles (including spherules of various sizes, and Ni-Cr spinels) as a consequence of the impact emplacement process inside the atmosphere and the water column.

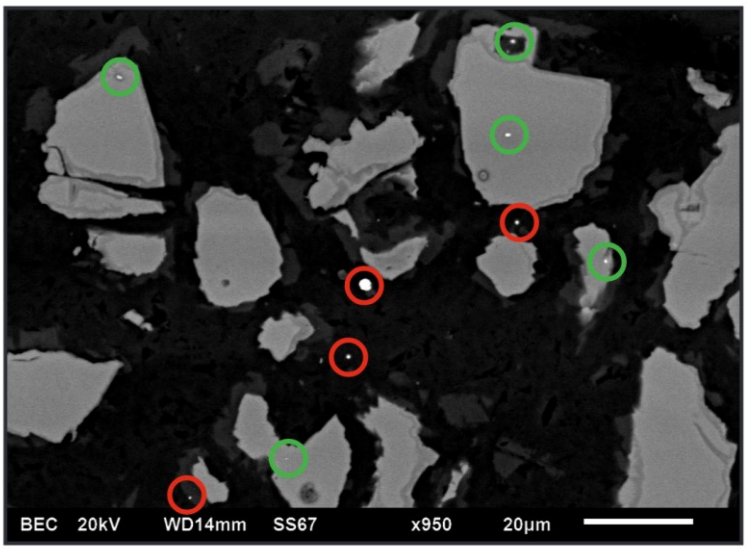

Figure 8. *Backscattered electron image of Ni-rich Cr spinels (grey) with the two PGE hosting phases, primary PGE metal alloy within unaltered spinels (green circles) and secondary PGE sulfarsenides within the matrix (red circles) (from Mohr-Westheide et al., 2015).*

Notably, the results obtained in this study confirm the observations and interpretations drawn by Mohr-Westheide et al. (2015) and Fritz et al. (2016) in that the extraterrestrial admixture can be found in both reservoirs (spherules and groundmass). The matrix separate from this study exhibits consistently higher PGE concentrations than the spherule sample (e.g., ~171 ppb Os compared to ~84 ppb, ~205 ppb Ir compared to ~70 ppb, and ~595 ppb Pt compared to ~185 ppb; see Table 1 and Result chapter for detailed comparison). Figure 9 also visualizes the relationship between all analyzed separates for the HSE abundances. Compared to non-impact-related Fig Tree sediments, all samples have elevated PGE abundances, arguing for substantial meteoritic admixtures within the groundmass (shale matrix) and the spherules. The PGE abundance data can best be interpreted by assuming that there is a higher concentration of meteoric carrier phase(s) in the matrix compared to the spherules. Furthermore, the secondary alteration must have affected all PGE to the same extent, as both separates and the mix show linear correlation for Ir vs. Os, Pt vs. Os. and Pt vs. Ir plots. On the other hand, Re was affected more than the PGEs and shows no correlation for the Re vs. Os plot.

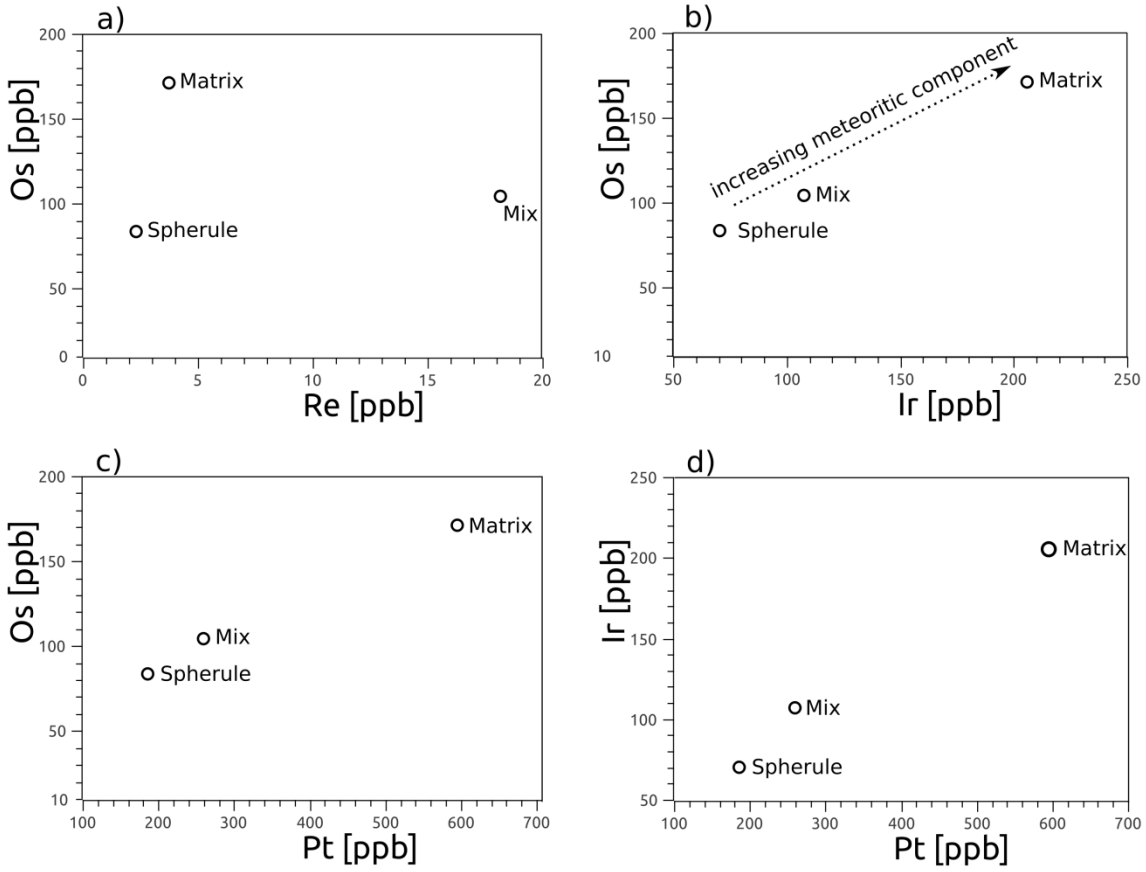

Figure 9. *Interelement plots of the abundances of Re vs. Os, Ir vs. Os, Pt vs. Os. and Pt vs. Ir for all analyzed samples.*

In contrast to the varying PGE abundances between the spherule and matrix separate, the $^{187}Os/^{188}Os$ isotope compositions vary much less (~0.1077 vs. ~0.1058, respectively). Such a trend indicates that, regardless of the total content, all osmium in the separates is of meteoritic origin. The only lithology exhibiting similarly low $^{187}Os/^{188}Os$ isotope compositions are ultramafic rocks like komatiites (Puchtel et al., 2009, 2014; Connolly et al., 2011). However, as discussed by Schulz et al. (2017), these rocks can be excluded as a source of Os due to their distinct Cr/Ir ratios, their total HSE abundances (up to three orders of magnitude lower compared to the BARB5 spherule samples), and the geological context (of Fig Tree group hosted spherule layers unrelated to komatiites, which are predominantly present in the older Onverwacht group; e.g., Hofmann, 2005; Anhaeusser, 2014). Thus, only a minor part of the meteoritic carrier phase is incorporated in the spherules, while most of it is distributed in the matrix.

This finding (of spherule related and spherule-unrelated meteoritic components found on the basis of bulk geochemical data from hand-picked separates), in conjunction with

the earlier published in-situ investigations by Mohr-Westheide et al. (2015), has direct implications for the understanding of the interplay between vaporization, condensation, and Ni-Cr spinel and spherule genesis inside the impact vapor plume and the concurrent impact emplacement process (but a detailed evaluation of these topics is beyond the scope of this bachelor thesis).

4.2 The rhenium problem

The $^{187}Os/^{188}Os$ isotope composition is a function of time elapsed since the closure of the system for Re and Os and the Re/Os ratio. The higher the Re/Os ratio, the more ^{187}Os is produced via radioactive decay of ^{187}Re in a given timespan, resulting in increased $^{187}Os/^{188}Os$ isotope ratios. Samples with chondritic HSE admixture are supposed to follow the chondritic evolution line. If, however, the Re/Os ratio is changed through gain or loss of Re or Os, the evolution line of the sample also differs from the chondritic evolution, which can be equated with the evolution of the primitive mantle (e.g., Faure, 1986) (see Fig. 10). Any partial melting events (e.g., the generation of the UCC through time) will, due to the more incompatible behavior of Re, lead to ever increasing Re/Os ratios within the partial melts (leaving behind a complementary residual reservoir). Therefore, Fig Tree sediments and all other crustal lithologies exhibit comparably radiogenic $^{187}Os/^{188}Os$ ratios (the average UCC has an $^{187}Os/^{188}Os$ of ~1.05 ± 0.23; Peucker-Ehrenbrink et al. 2001).

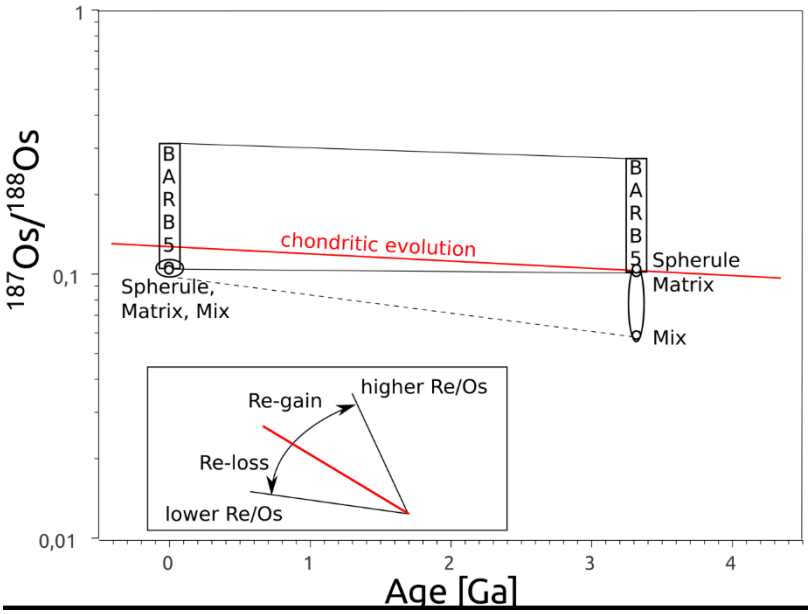

***Figure 10**. Evolution of the $^{187}Os/^{188}Os$ isotope system showing the range of initial and present day $^{187}Os/^{188}Os$ ratios for BARB5 samples (rectangles) (Schulz et al., 2017) and for spherule sample, matrix separate and mix of this study (ellipses). The red line represents the chondritic evolution (Shirey and Walker, 1998).*

Using the Re/Os ratio and the present-day $^{187}Os/^{188}Os$ isotope ratio, the initial $^{187}Os/^{188}Os$ isotope ratio can be back-calculated. This initial isotope ratio is fictive, but if it is geologically meaningful (in case of impactites, chondritic or superchondritic) it can be assumed as real.

Schulz et al. (2017) back-calculated the isotope compositions of all BARB5 spherule layer samples to the approximate time of impact (~3.32 Ga ago; Lowe and Byerly, 1999) and consistently yielded either chondritic values (back- calculated to the time of impact 3.32 Ga ago, chondrites had a $^{187}Os/^{188}Os$ isotope ratio of ~0.1048; Shirey and Walker, 1998) or superchondritic ratios (see Fig. 10). Subchondritic present-day (measured) $^{187}Os/^{188}Os$ isotope compositions of spherule layers C to E in the BARB5 drill core section were explained by Re- loss through selective volatilization of rhenium in the wake of the impact (Schulz et al., 2017). This would result in an isotopic evolution of the spherule layer samples with subchondritic Re/Os ratios, ultimately resulting in subchondritic present-day $^{187}Os/^{188}Os$ isotope signatures. However, selective volatilization is unlikely since Os and Re have very similar condensation temperatures (Lodders, 2003), and it must have been a process during which Re is affected differently than Os. So selective mobilization of Re during hydrothermal alteration or metamorphosis is much more likely as Re is more fluid mobile than Os (e.g., Sun et al., 2004) and there is mineralogical evidence for (minor) secondary alteration (Mohr-Westheide et al., 2015; Fritz et al., 2016).

The present day $^{187}Os/^{188}Os$ isotope ratios of the samples analyzed in this study are, in part, less radiogenic than the most unradiogenic present-day $^{187}Os/^{188}Os$ ratios measured for BARB5 samples by Schulz et al. (2017). Back-calculated to the time of impact, the matrix separate and the mixed sample from this study yield, in marked contrast to the results obtained in earlier studies of spherule-groundmass assemblages, subchondritic initial values, ranging between 0.0593 ± 0.0018 to 0.1018 ± 0.0031 for mix and the matrix separate, respectively. The spherule sample has an initial $^{87}Os/^{188}Os$ ratio of 0.1058 ± 0.0032 and is therefore slightly above the chondritic value (see Fig. 10). The back-calculated value of 0.0593 ± 0.0018, for the mixed sample is geologically meaningless, exemplifying that initial $^{187}Os/^{188}Os$ ratios of BARB5 samples provide no tool to draw any conclusions on the impactor type (see Fig. 10). It is, however, difficult to reconcile, based on the data for three separates, which processes account for the subchondritic initial values obtained in this study. A difficult interplay of loss and gain of (fluid-mobile; e.g., Sun et al., 2004) rhenium during (possible multiple) hydrothermal overprints for these isotope signatures, which obscure the initial meteoritic signal.

4.3 Conclusions

The sample from layer E of the BARB5 spherule layer section (Barberton Greenstone Belt, South Africa) was separated into a highly spherule-enriched separate (> ~95% spherules), a highly spherule-depleted groundmass separate (< ~5% spherules), and a mixed sample of remixed, not separable components. Highly siderophile element concentrations of the separates are up to three orders of magnitude higher than non-impact related sediments of the Fig Tree Group (graywackes, metapelites, siltstones, and black shales) and provide evidence for (i) substantial meteoritic admixtures, (ii) occurrence of meteoritic components in spherules and the shaly matrix, and (iii) higher concentrations of meteoritic carrier phases in the matrix compared to the spherule separate. Furthermore, near chondritic Os/Ir ratios strengthen the impact hypothesis. The subchondritic $^{187}Os/^{188}Os$ isotope ratios of the analyzed separates count among the least radiogenic values of the BARB5 spherule layer section. In contrast to Ir vs. Os, Pt vs. Os. and Pt vs. Ir, the Re vs. Os plot lacks linear correlation and indicates, together with a geologically meaningless, extremely low, subchondritic initial $^{187}Os/^{188}Os$ isotope ratio for the mixed sample, that the Re system has been disturbed, most probably by selective mobilization of Re through hydrothermal overprints.

Bibliography

Anhaeusser, C. R. (2014). Archaean greenstone belts and associated granitic rocks–a review. *Journal of African Earth Sciences*, ***100***, 684-732.

Botha A. (2010) The quantitative characterisation of geological reference materials by isotope dilution inductively coupled plasma mass spectrometry (ICP-MS) *Doctoral dissertation*, University of Pretoria, Pretoria, 30-42

Bottke, W. F., Vokrouhlický, D., Minton, D., Nesvorný, D., Morbidelli, A., Brasser, R., Simonson, B., & Levison, H. F. (2012). An Archaean heavy bombardment from a destabilized extension of the asteroid belt. *Nature*, ***485***, 78.

Brandon, A. D., Humayun, M., Puchtel, I. S., Leya, I., & Zolensky, M. (2005). Osmium isotope evidence for an s-process carrier in primitive chondrites. *Science*, ***309***, 1233-1236.

Burnham M., Meisel T., & Kriete C. 2010. OKUM and MUH-1: Two new IAG-certified ultramafic rock reference materials (abstract). *Geochimica et Cosmochimica Acta, **74***, Supplement 129.

Chu, Z., Yan, Y., Chen, Z., Guo, J., Yang, Y., Li, C., & Zhang, Y. (2015). A comprehensive method for precise determination of Re, Os, Ir, Ru, Pt, Pd concentrations and Os isotopic compositions in geological samples. *Geostandards and Geoanalytical Research*, ***39***, 151-169.

Cohen, A. S., & Waters, F. G. (1996). Separation of osmium from geological materials by solvent extraction for analysis by thermal ionisation mass spectrometry. *Analytica Chimica Acta*, ***332***, 269-275.

Connolly, B. D., Puchtel, I. S., Walker, R. J., Arevalo, R., Piccoli, P. M., Byerly, G., Robin-Popioul, C., & Arndt, N. (2011). Highly siderophile element systematics of the 3.3 Ga Weltevreden komatiites, South Africa: implications for early Earth history. *Earth and Planetary Science Letters*, ***311***, 253-263.

Creaser, R. A., Papanastassiou, D. A., & Wasserburg, G. J. (1991). Negative thermal ion mass spectrometry of osmium, rhenium and iridium. *Geochimica et Cosmochimica Acta*, ***55***, 397-401.

Dietz R. S. (1968) In *Shock metamorphism of natural materials*, French B. M. & Short N. M., Eds, Baltimore: Mono Book Corporation. pp. 267–285.

Dietz, R. S. (1959). Shatter cones in cryptoexplosion structures (meteorite impact?). *The Journal of Geology*, ***67***, 496-505.

Dietz, R. S. (1963a). Cryptoexplosion structures; a discussion. *American Journal of Science*, ***261***, 650-664.

Dietz, R. S. (1963b). Astroblemes: Ancient meteorite-impact structures on the Earth. *The Moon Meteorites and Comets*, Middlehurst, B.M. & Kuiper, G.P., Eds, Chicago: University of Chicago Press. p. 285.

Earth Impact Database (2017) <http://www.unb.ca/passc/ImpactDatabase/> (accessed: 16th August, 2017)

Encyclopædia Britannica (2017) <> (accessed: 16th August, 2017)

Evans, N. J., Gregoire, D. C., & Goodfellow, W. D. (1993). Use of platinum-group elements for impactor identification: Terrestrial impact craters and Cretaceous-Tertiary boundary. *Geochimica et Cosmochimica Acta*, ***57***, 3737-3748.

Faure G. (1986). In Principles of Isotope Geology, 2nd edition., Faure, G., Eds, New York: Wiley. pp. 341–361.

French, B. M., & Koeberl, C. (2010). The convincing identification of terrestrial meteorite impact structures: What works, what doesn't, and why. *Earth-Science Reviews*, ***98***, 123-170.

Fritz, J., Tagle, R., Ashworth, L., Schmitt, R. T., Hofmann, A., Luais, B., Harris, P. D., & Koeberl, C. (2016). Nondestructive spectroscopic and petrochemical investigations of Paleoarchean spherule layers from the ICDP drill core BARB5, Barberton Mountain Land, South Africa. *Meteoritics & Planetary Science*, ***51***, 2441-2458.

Glass, B. (1967). Microtektites in deep-sea sediments. *Nature*, ***214***, 372-374.

Glass B. P., & Simonson, B. M. (2013). Distal Impact Ejecta Layers: A Record of Large Impacts in Sedimentary Deposits. *Elements, **8,*** 43-48

Goderis, S., Simonson, B. M., McDonald, I., Hassler, S. W., Izmer, A., Belza, J., Terryn, H., Vahaecke, F., & Claeys, P. (2013). Ni-rich spinels and platinum group element nuggets condensed from a late Archaean impact vapour cloud. *Earth and Planetary Science Letters*, ***376***, 87-98.

Hassler, S. W., & Simonson, B. M. (2001). The sedimentary record of extraterrestrial impacts in deep-shelf environments: Evidence from the early Precambrian. *The Journal of Geology*, ***109***, 1-19.

Heubeck, C., Engelhardt, J., Byerly, G. R., Zeh, A., Sell, B., Luber, T., & Lowe, D. R. (2013). Timing of deposition and deformation of the Moodies Group (Barberton Greenstone Belt, South Africa): Very-high-resolution of Archaean surface processes. *Precambrian Research*, ***231***, 236-262.

Ishikawa A., Senda R., Suzuki K., Dale C. W., & Meisel T. (2014). Re-evaluating digestion methods for highly siderophile element and ^{187}Os isotope analysis: Evidence from geological reference materials. *Chemical Geology,* ***384***, 27–46.

Johnson, B. C., & Melosh, H. J. (2012). Formation of spherules in impact produced vapor plumes. *Icarus*, ***217***, 416-430.

Johnson S. F., Reimold, W. U., Koeberl, C., & Mcdonald, I. (1999). Early Archean Spherule Beds in the Barberton Mountain Land, South Africa: Impact or Terrestrial Origin? *Meteoritics & Planetary Science,* ***34***, 59-60.

Kamo, S. L., Reimold, W. U., Krogh, T. E., & Colliston, W. P. (1996). A 2.023 Ga age for the Vredefort impact event and a first report of shock metamorphosed zircons in pseudotachylitic breccias and granophyre. *Earth and Planetary Science Letters*, ***144***, 369-387.

Koeberl, C. (2003). The Late Heavy Bombardment in the inner solar system: Is there any connection to Kuiper belt objects?. *Earth, Moon, and Planets*, ***92***, 79-87.

Koeberl, C. (2006). The record of impact processes on the early Earth: A review of the first 2.5 billion years. *Geological Society of America Special Papers*, ***405***, 1-22.

Koeberl, C., (2014). The geochemistry and cosmochemistry of impacts. In, **Vol. 2** (ed. A. Davis), *Treatise on Geochemistry* (Second Edition). Holland, H., & Turekian, K., Eds, Oxford: Elsevier Ltd. pp. 73–118.

Koeberl, C., & Reimold, W. U. (1994). Archean spherule beds: Impact or terrestrial origin? Reply to the comment by A. Glikson. *Earth and Planetary Science Letters*, ***126***, 497-499.

Koeberl, C., & Reimold, W. U. (1995). Early Archaean spherule beds in the Barberton Mountain Land, South Africa: no evidence for impact origin. *Precambrian Research*, ***74***, 1-33.

Koeberl, C., Reimold, W. U., & Boer, R. H. (1993). Geochemistry and mineralogy of Early Archean spherule beds, Barberton Mountain Land, South Africa: Evidence for origin by impact doubtful. *Earth and planetary science letters*, ***119***, 441-452.

Kong, P., Ebihara, M., & Nakahara, H. (1996). Determination of 18 siderophile elements including all platinum group elements in chondritic metals and iron meteorites by instrumental neutron activation. *Analytical chemistry*, ***68***, 4130-4134.

Kyte, F. T., Shukolyukov, A., Lugmair, G. W., Lowe, D. R., & Byerly, G. R. (2003). Early Archean spherule beds: Chromium isotopes confirm origin through multiple impacts of projectiles of carbonaceous chondrite type. *Geology*, ***31***, 283-286.

Lodders K. (2003). Solar system abundances and condensation temperatures of the elements. *Astrophysical Journal,* **591**, 1220–1247.

Lowe, D. R., & Byerly, G. R. (1986). Early Archean silicate spherules of probable impact origin, South Africa and Western Australia. *Geology*, ***14***, 83-86.

Lowe, D. R., & Byerly, G. R. (1999). Stratigraphy of the west-central part of the Barberton Greenstone Belt, South Africa. In *Geologic evolution of the Barberton Greenstone Belt, South Africa*. Lowe, D. R., & Byerly, G. R., Eds, GSA Special Paper 329. Boulder, Colorado: Geological Society of America. pp. 1-36.

Lowe D.R. & G.R. Byerly (2007). Geology of the Barberton Greenstone Belt, South Africa. In *Earth's Oldest Rocks*, van Kranendonk, M., Eds, Oxford: Elsevier. p.481-526.

Lowe, D. R., Byerly, G. R., Kyte, F. T., Shukolyukov, A., Asaro, F., & Krull, A. (2003). Spherule beds 3.47–3.24 billion years old in the Barberton Greenstone Belt, South Africa: a record of large meteorite impacts and their influence on early crustal and biological evolution. *Astrobiology*, ***3***, 7-48.

Luguet, A., Nowell, G. M., & Pearson, D. G. (2008). ^{184}Os/^{188}Os and ^{186}Os/^{188}Os measurements by Negative Thermal Ionisation Mass Spectrometry (N-TIMS): effects of interfering element and mass fractionation corrections on data accuracy and precision. *Chemical Geology*, ***248***, 342-362.

Luguet, A., Behrens, M., Pearson, D. G., König, S., & Herwartz, D. (2015). Significance of the whole rock Re–Os ages in cryptically and modally metasomatised cratonic peridotites: Constraints from HSE–Se–Te systematics. *Geochimica et Cosmochimica Acta*, ***164***, 441-463.

Meisel, T., Walker, R. J., Irving, A. J., & Lorand, J. P. (2001). Osmium isotopic compositions of mantle xenoliths: a global perspective. *Geochimica et Cosmochimica Acta*, ***65***, 1311-1323.

Meisel T., Burnham O. M., Kriete C., Syed N., Bokhari H., & Schulz T. 2013. Osmium isotope and PGE reference materials OKUM and MUH-1 (abstract*). Mineralogical Magazine, **77***, 1734.

Milton, D. J. (1977). Shatter cones-an outstanding problem in shock mechanics. In *Impact and Explosion Cratering: Planetary and Terrestrial Implications* Roddy, D.J., Pepin, R.O., & Merill, R.P., Eds, New York: Pergamon Press. pp. 703-714.

Mohr-Westheide, T., Reimold, W. U., Fritz, J., Koeberl, C., Salge, T., Hofmann, A., & Schmitt, R. T. (2015). Discovery of extraterrestrial component carrier phases in Archean spherule layers: Implications for estimation of Archean bolide sizes. *Geology*, ***43***, 299-302.

Mougel, B., Moynier, F., Göpel, C., & Koeberl, C. (2017). Chromium isotope evidence in ejecta deposits for the nature of Paleoproterozoic impactors. *Earth and Planetary Science Letters*, ***460***, 105-111.

Melosh HJ. (1989). Impact Cratering – A Geologic Process, Melosh, H.J., Eds, New York: Oxford University Press, pp. 245., Ozdemir, S., Schulz, T., Koeberl, C., Reimold, W. U., Mohr-Westheide, T., & Hofmann, A. (2016). Paleoarchean Spherule Beds in the CT3 Drill Core from the Barberton Greenstone Belt, South Africa: Geochemistry and Os Isotopic Signatures. *Meteoritics & Planetary Science, **51**, 503-566*.

Palme, H., Janssens, M. J., Takahashi, H., Anders, E., & Hertogen, J. (1978). Meteoritic material at five large impact craters. *Geochimica et Cosmochimica Acta*, ***42***, 313-323.

Peucker-Ehrenbrink, B., & Jahn, B. M. (2001). Rhenium-osmium isotope systematics and platinum group element concentrations: Loess and the upper continental crust. *Geochemistry, Geophysics, Geosystems*, ***2***, doi:10.1029/2001GC000172.

Puchtel, I. S., Walker, R. J., Anhaeusser, C. R., & Gruau, G. (2009). Re–Os isotope systematics and HSE abundances of the 3.5 Ga Schapenburg komatiites, South Africa: Hydrous melting or prolonged survival of primordial heterogeneities in the mantle?. *Chemical Geology*, ***262***, 355-369.

Puchtel, I. S., Walker, R. J., Touboul, M., Nisbet, E. G., & Byerly, G. R. (2014). Insights into early Earth from the Pt–Re–Os isotope and highly siderophile element abundance systematics of Barberton komatiites. *Geochimica et Cosmochimica Acta*, ***125***, 394-413.

Rasmussen, B., & Koeberl, C. (2004). Iridium anomalies and shocked quartz in a Late Archean spherule layer from the Pilbara craton: New evidence for a major asteroid impact at 2.63 Ga. *Geology*, ***32***, 1029-1032.

Reimer, T. O. (1983). Pseudo-oolites in rocks of the Ulundi Formation, lower part of the Archaean Fig Tree Group (South Africa). *Precambrian Research*, ***20***, 375-390.

Roy-Barman, M., & Allègre, C. J. (1995). ^{187}Os/^{186}Os in oceanic island basalts: tracing oceanic crust recycling in the mantle. *Earth and Planetary Science Letters*, ***129***, 145-161.

Ryder, G. (1990). Lunar samples, lunar accretion and the early bombardment of the Moon. *Eos, Transactions American Geophysical Union*, ***71***, 313-323.

Ryder G. (2001). Mass flux during the ancient lunar bombardment: The cataclysm. *Lunar and Planetary Science, **32***, Abstract No. 1326 (CD-ROM)

Ryder G. (2002). Mass flux in the ancient Earth–Moon system and benign implications for the origin of life on Earth. *Journal of Geophysical Research,* **107**, 6-1–6-14.

Schulz, T., Luguet, A., Wegner, W., Acken, D., & Koeberl, C. (2016). Target rocks, impact glasses, and melt rocks from the Lonar crater, India: Highly siderophile element systematics and Sr-Nd-Os isotopic signatures. *Meteoritics & Planetary Science*, ***51***, 1323-1339.

Schulz, T., Koeberl, C., Luguet, A., van Acken, D., Mohr-Westheide, T., Ozdemir, S., & Reimold, W. U. (2017). New constraints on the Paleoarchean meteorite bombardment of the Earth–Geochemistry and

Re-Os isotope signatures of spherule layers in the BARB5 ICDP drill core from the Barberton Greenstone Belt, South Africa. *Geochimica et Cosmochimica Acta*, ***211***, 322-340.

Shen, J. J., Papanastassiou, D. A., & Wasserburg, G. J. (1996). Precise Re□ Os determinations and systematics of iron meteorites. *Geochimica et Cosmochimica Acta*, ***60***, 2887-2900.

Shirey, S. B., & Walker, R. J. (1998). The Re-Os isotope system in cosmochemistry and high-temperature geochemistry. *Annual Review of Earth and Planetary Sciences*, ***26***, 423-500.

Shukolyukov, A., & Lugmair, G. (1998). Isotopic evidence for the Cretaceous-Tertiary impactor and its type. *Science*, ***282***, 927-930.

Shukolyukov A., Castillo P., Simonson B.M., & Lugmair G.W. (2002). Chromium in late Archean spherule layers from Hamersley basin, Western Australia: isotopic evidence for extraterrestrial component. *Lunar and Planetary Science, **33***, 13-69.

Siebert, C., Kramers, J. D., Meisel, T., Morel, P., & Nägler, T. F. (2005). PGE, Re-Os, and Mo isotope systematics in Archean and early Proterozoic sedimentary systems as proxies for redox conditions of the early Earth. *Geochimica et Cosmochimica Acta*, ***69***, 1787-1801.

Simonson, B. M. (1992). Geological evidence for a strewn field of impact spherules in the early Precambrian Hamersley Basin of Western Australia. *Geological Society of America Bulletin*, ***104***, 829-839.

Simonson, B. M. (2003). Petrographic criteria for recognizing certain types of impact spherules in well-preserved Precambrian successions. *Astrobiology*, ***3***, 49-65.

Simonson, B. M., Schubel, K. A., & Hassler, S. W. (1993). Carbonate sedimentology of the early Precambrian Hamersley Group of western Australia. *Precambrian Research*, ***60***, 287-335.

Simonson, B. M., & Hassler, S. W. (1997). Revised correlations in the early Precambrian Hamersley Basin based on a horizon of resedimented impact spherules. *Australian Journal of Earth Sciences*, ***44***, 37-48.

Simonson, B. M., Davies, D., Wallace, M., Reeves, S., & Hassler, S. W. (1998). Iridium anomaly but no shocked quartz from Late Archean microkrystite layer: Oceanic impact ejecta?. *Geology*, ***26***, 195-198.

Smoliar M.I., R.J. Walker, J.W. Morgan (1996). Re-Os ages of Group IIA, IIIA, IVA, and IVB iron meteorites. *Science, **271***, 1099–102

Sun, W., Bennett, V. C., & Kamenetsky, V. S. (2004). The mechanism of Re enrichment in arc magmas: evidence from Lau Basin basaltic glasses and primitive melt inclusions. *Earth and Planetary Science Letters*, ***222***, 101-114.

Stöffler, D., & Grieve, R. A. F. (2007). Impactites. In *Metamorphic rocks: A classification and glossary of terms, recommendations of the International Union of Geological Sciences*, Fette, D., & Desmons, P., Eds, Cambridge: Cambridge University Press, pp. 82-92.

Tagle, R., & Berlin, J. (2008). A database of chondrite analyses including platinum group elements, Ni, Co, Au, and Cr: Implications for the identification of chondritic projectiles. *Meteoritics & Planetary Science*, ***43***, 541-559.

van Acken, D., Brandon, A. D., & Humayun, M. (2011). High-precision osmium isotopes in enstatite and Rumuruti chondrites. *Geochimica et Cosmochimica Acta*, ***75***, 4020-4036.

Vogl, J., & Pritzkow, W. (2010). Isotope dilution mass spectrometry—a primary method of measurement and its role for RM certification. *Mapan- Journal of Metrology Society of India, **25***, 135-164.

Völkening, J., Walczyk, T., & Heumann, K. G. (1991). Osmium isotope ratio determinations by negative thermal ionization mass spectrometry. *International Journal of Mass Spectrometry and Ion Processes*, ***105***, 147-159.

Woodhead, J. D., Hergt, J. M., & Simonson, B. M. (1998). Isotopic dating of an Archean bolide impact horizon, Hamersley Basin, Western Australia. *Geology*, ***26***, 47-50.

List of figures

Figure 1. Histogram of ages of known terrestrial impact structures, exemplifying the crater age bias towards the last 500 Ma. The dot-pattern indicates impact structures, whereas the hatched pattern signifies ejecta layers (from Koeberl, 2006). 4

Figure 2. Classification scheme of impactites (after Stöffler and Grieve, 2007). 7

Figure 3. Range of Iridium contents in various terrestrial materials compared to chondrites. All other HSE (except Re) follow a similar trend (from Koeberl, 1998). 10

Figure 4a and **4b** ^{187}Os isotopic ratios vs. Os content and Re-Os isotopic diagram used as mixing diagrams between meteorites and target rocks. Impactites plot between the two endmembers (from Koeberl, 2014). 11

Figure 5. Stratigraphic column of the BARB5 drill core from 517 to 503 m through the spherule-bearing core interval (left) and cross section of the spherule layer section (511.51 to 511.29 m), showing the B-E spherule layers in the BARB5 drill core (right). Numbers refer to depth in meters in the core. Layer E-20, analyzed in this study, is highlighted (blue rectangle). (modified from Fritz et al., 2016; Schulz et al., 2017). 13

Figure 6. Workflow scheme outlining and sketching all steps of sample preparation and analytical methods applied in this study. 15

Figure 7. Osmium vs. Ir abundance plot for samples of this study and for BARB5 spherule layer section compared to Fig Tree Group sediments, and chondrites. All samples plot along the mixing line between chondrites and Fig Tree Group Sediments (i.e., crustal target rocks). (° Siebert et al., 2005; [x] Tagle and Berlin, 2008; * Schulz et al., 2017) 23

Figure 8. Backscattered electron image of Ni-rich Cr spinels (grey) with the two PGE hosting phases, primary PGE metal alloy within unaltered spinels (green circles) and secondary PGE sulfarsenides within the matrix (red circles) (from Mohr-Westheide et al., 2015). 24

Figure 9. Interelement plots of the abundances of Re vs. Os, Ir vs. Os, Pt vs. Os. and Pt vs. Ir for all analyzed samples. 25

Figure 10. Evolution of the $^{187}Os/^{188}Os$ isotope system showing the range of initial and present day $^{187}Os/^{188}Os$ ratios for BARB5 samples (rectangles) (Schulz et al., 2017) and for spherule sample, matrix separate and mix of this study (ellipses). The red line represents the chondritic evolution (Shirey and Walker, 1998). 26

List of tables

Table 1. Concentrations (in ppb) of Re, Os Ir, and Pt, Os/Ir ratios, and $^{187}Os/^{188}Os$, $^{187}Re/^{188}Os$, and initial $^{187}Os/^{188}Os$ isotope ratios, the latter back-calculated to the age of middle Mapepe formation (3.32 Ga; Lowe and Byerly, 1999), measured in this study for separates from layer E of the BARB5 spherule layer, as well as data for other BARB5 spherule layers, Fig Tree Group sediments, and chondrites. Data from this sample are in bold. ([x] Shirey and Walker 1998; ° Siebert et al., 2005; Tagle and Berlin, 2008; *Schulz et al., 2017) 20

Appendix

Meteoritic admixture to BARB5- layers B to E

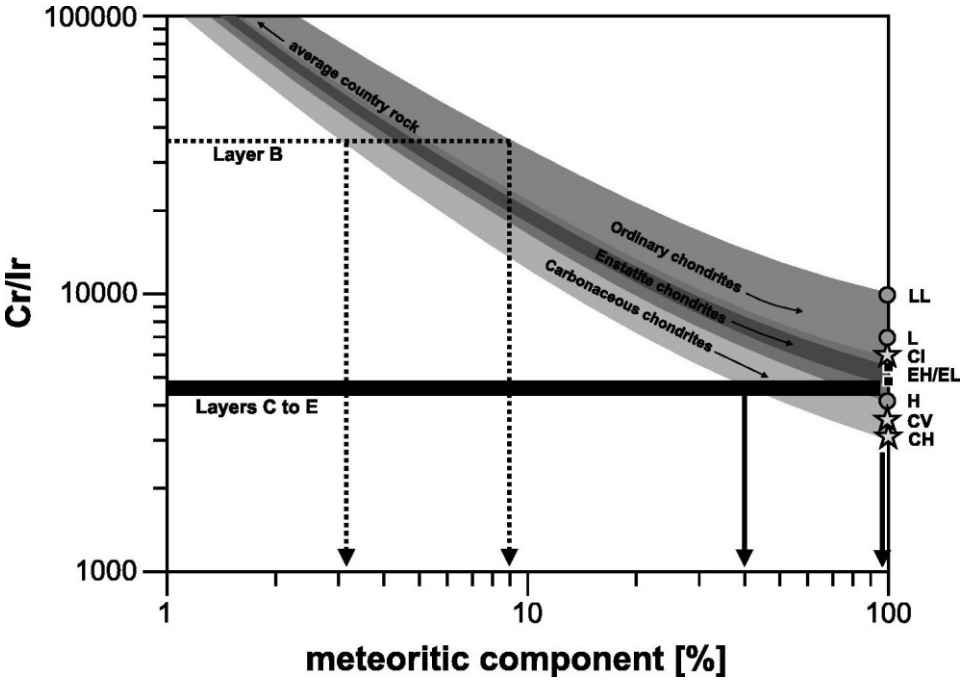

***Figure A1**. Diagram showing the magnitude of meteoritic component in BARB5- layers B to E based on the minimum measured Cr/Ir ratio of the layers. The magnitude of meteoritic admixture also depends on the assumed type of chondrite (from Schulz et al., 2017).*

Equation for isotope dilution

$$C_x = \left(\frac{C_s W_s}{W_x}\right) * \left(\frac{A_s - R_m B_s}{R_m B_x - A_x}\right)$$

where

A_x , B_x = the atom fractions of isotopes A and B in the sample, relative to all isotopes

A_s , B_s = the atom fractions of isotopes A and B in the spike

C_x , C_s = the elemental mass concentrations in the sample and the spike, respectively

R_m =measured isotope ratio

W_x , W_s = the weights of the sample and the spike, respectively

(Botha, 2010)

HSE column chemistry

Table A1. *Steps and eluents used for the HSE column chemistry.*

1. Stage		2. Stage	
Elution	**Step**	**Elution**	**Step**
10 ml H_2O	Resin cleaning	4 ml H_2O	Resin cleaning
10 ml 6 mol/l HNO_3	Resin cleaning	4 ml 6 mol/l HCl twice	Resin cleaning
10 ml conc. HNO_3	Resin cleaning	4 ml 6 mol/l HF	Resin cleaning
2 ml H_2O	Resin cleaning	4 ml 6 mol/l HCl	Resin cleaning
10 ml conc. HCl	Resin cleaning	4 ml 6 mol/l HF	Resin cleaning
2 ml H_2O	Resin cleaning	4 ml H_2O	Resin cleaning
2 ml 1 mol/l HCl twice	Equilibration	4 ml 1 mol/l HCl	Equilibration
10 ml 1 mol/l HCl	Load sample	1 ml 1 mol/l HCl	Load and collect Pd
5 ml 1 mol/l HCl	Rinse matrix	4 ml 1 mol/l HCl	Collect Pd
2 ml 0.8 mol/l HNO_3 twice	Rinse matrix	1 ml 1 mol/l HCl	Load and collect Ru-Re-Ir-Pt
15 ml conc. HNO_3	Collect Ru-Re-Ir-Pt	5 ml 1 mol/l HCl	Collect Ru-Re-Ir-Pt
2 ml H_2O	Rinse HNO_3	4 ml 2 mol/l HF twice	Resin cleaning
15 ml conc. HCl	Collect Pd	4 ml 6 mol/l HCl	Resin cleaning
10 ml conc. HCl	Collect Pd	4 ml 2 mol/l HF	Resin cleaning
10 ml conc. HCl	Collect Pd	4 ml 6 mol/l HCl	Resin cleaning

Modified from Chu et al., 2014

Calculation of the amount of PGE-carrier phase

According to Mohr-Westheide et al. (2015) the PGE alloy comprise ~40 at% Ni, ~40 at% Pt metal alloyed with minor amounts of Ir, Os, Ru, Pd, and/or Rh, and Fe. So the chemical formula would be Pt_2Ni_2(Ir,Os,Ru,Pd,Rh,Fe) and the molar mass (M_{tot}) ~650 g/mol. The weight percentage of Pt would be ~60 w% ($w\%(Pt) = \frac{2*M(Pt)}{M_{tot}}$).

The BARB5 spherule layers contain 5,2 to 2082 ppb Pt. Since the sample splits had ~200 mg, they hold ~$1.04*10^{-6}$ to ~$416*10^{-6}$ mg Pt. To get this mass, ~$1.73*10^{-6}$ to ~$693*10^{-6}$ mg of the PGE alloy are needed, this would be ~8.56 to ~3470 ppb (~0.000000856 to ~0.000347 w%) PGE alloy.

Mass interferences on Os

Table A2*. Possible mass interferences for OsO_3^-, which was measured in this study via N-TIMS.*

Mass	Os	Re	O	O	O
232	184		16	16	16
233	184		16	16	17
233		185	16	16	16
234	184		16	17	17
234	184		16	16	18
234		185	16	16	17
234	186		16	16	16
235	184		17	17	17
235	184		16	17	18
235		185	16	17	17
235		185	16	16	18
235	186		16	16	17
235	187		16	16	16
236	184		16	18	18
236	184		17	17	18
236		185	17	17	17
236		185	16	17	18
236	186		16	17	17
236	186		16	16	18
236	187		16	16	17
236	188		16	16	16
237	184		17	18	18
237		185	16	18	18
237		185	17	17	18
237	186		17	17	17
237	186		16	17	18
237	187		16	17	17
237	187		16	16	18
237	188		16	16	17
237	189		16	16	16
238	184		18	18	18
238		185	17	18	18
238	186		16	18	18
238	186		17	17	18
238	187		17	17	17
238	187		16	17	18
238	188		16	17	17
238	188		16	16	18
238	189		16	16	17
238	190		16	16	16
239		185	18	18	18

239	186	17	18	18
239	187	16	18	18
239	187	17	17	18
239	188	17	17	17
239	188	16	17	18
239	189	16	17	17
239	189	16	16	18
239	190	16	16	17
240	186	18	18	18
240	187	17	18	18
240	188	16	18	18
240	188	17	17	18
240	189	17	17	17
240	189	16	17	18
240	190	16	17	17
240	190	16	16	18
240	192	16	16	16
241	187	18	18	18
241	188	17	18	18
241	189	16	18	18
241	189	17	17	18
241	190	17	17	17
241	190	16	17	18
241	192	16	16	17
242	188	18	18	18
242	189	17	18	18
242	190	16	18	18
242	190	17	17	18
242	192	16	17	17
242	192	16	16	18
243	189	18	18	18
243	190	17	18	18
243	192	17	17	17
243	192	16	17	18
244	190	18	18	18
244	192	16	18	18
244	192	17	17	18
245	192	17	18	18
246	192	18	18	18

(e.g., Shirey and Walker, 1998; Brandon et al., 2005)